Pergamon

Geochimica et Cosmochimica Acta, Vol. 68, No. 8, pp. 1923–1941, 2004

0016-7037/04 $30.00 + .00

doi:10.1016/j.gca.2003.10.026

Amoeboid olivine aggregates with low-Ca pyroxenes: A genetic link between refractory inclusions and chondrules?

ALEXANDER N. KROT,[1,*] MICHAIL I. PETAEV,[2] and HISAYOSHI YURIMOTO[3]

[1]Hawai'i Institute of Geophysics and Planetology, School of Ocean and Earth Science and Technology, University of Hawai'i at Manoa, Honolulu, HI 96822, USA
[2]Harvard-Smithsonian Center for Astrophysics and Department of Earth and Planetary Sciences, Harvard University, Cambridge, MA 02138, USA
[3]Department of Earth and Planetary Sciences, Tokyo Institute of Technology, Tokyo 152-8551, Japan

(*Received June* 12, 2003; *accepted in revised form October* 20, 2003)

Abstract—Amoeboid olivine aggregates (AOAs) in primitive (unmetamorphosed and unaltered) carbonaceous chondrites are uniformly ^{16}O-enriched ($\Delta^{17}O \sim -20‰$) and consist of forsterite ($Fa_{<2}$), FeNi-metal, and a refractory component (individual CAIs and fine-grained minerals interspersed with forsterite grains) composed of Al-diopside, anorthite, ±spinel, and exceptionally rare melilite ($Åk_{<15}$); some CAIs in AOAs have compact, igneous textures. Melilite in AOAs is replaced by a fine-grained mixture of spinel, Al-diopside, and anorthite. Spinel is corroded by anorthite or by Al-diopside. In ~10% of > 500 AOAs studied in the CR, CV, CM, CO, CH, CB, and ungrouped carbonaceous chondrites Acfer 094, Adelaide, and LEW85332, forsterite is replaced to a various degree by low-Ca pyroxene. There are three major textural occurrences of low-Ca pyroxene in AOAs: (i) thin (<10 μm) discontinuous layers around forsterite grains or along forsterite grain boundaries in AOA peripheries; (ii) haloes and subhedral grains around FeNi-metal nodules in AOA peripheries, and (iii) thick (up to 70 μm) continuous layers with abundant tiny inclusions of FeNi-metal grains around AOAs. AOAs with low-Ca pyroxene appear to have experienced melting of various degrees. In the most extensively melted AOA in the CV chondrite Leoville, only spinel grains are relict; forsterite, anorthite and Al-diopside were melted. This AOA has an igneous rim of low-Ca pyroxene with abundant FeNi-metal nodules and is texturally similar to Type I chondrules.

Based on these observations and thermodynamic analysis, we conclude that AOAs are aggregates of relatively low temperature solar nebular condensates originated in ^{16}O-rich gaseous reservoir(s), probably CAI-forming region(s). Some of the CAIs were melted before aggregation into AOAs. Many AOAs must have also experienced melting, but of a much smaller degree than chondrules. Before and possibly after aggregation, melilite and spinel reacted with the gaseous SiO and Mg to form Ca-Tschermakite ($CaAl_2SiO_6$)-diopside ($CaMgSi_2O_6$) solid solution and anorthite. Solid or incipiently melted olivine in some AOAs reacted with gaseous SiO in the CAI- or chondrule-forming regions to form low-Ca pyroxene: $Mg_2SiO_4 + SiO_{(g)} + H_2O_{(g)} = Mg_2Si_2O_6 + H_{2(g)}$. Some low-Ca pyroxenes in AOAs may have formed by oxidation of Si-bearing FeNi-metal: $Mg_2SiO_4 + Si_{(in\ FeNi)} + 2H_2O_{(g)} = Mg_2Si_2O_6 + 2H_{2(g)}$ and by direct gas-solid condensation: $Mg_{(g)} + SiO_{(g)} + H_2O_{(g)} = Mg_2Si_2O_{6(s)} + H_{2(g)}$ from fractionated (Mg/Si ratio < solar) nebular gas.

Although bulk compositions of AOAs are rather similar to those of Type I chondrules, on the projection from spinel onto the plane Ca_2SiO_4-Mg_2SiO_4-Al_2O_3, these objects plot on different sides of the anorthite-forsterite thermal divide, suggesting that Type I chondrules cannot be produced from AOAs by an igneous fractionation. Formation of low-Ca pyroxene by reaction of AOAs with gaseous SiO and by melting of silica-rich dust accreted around AOAs moves bulk compositions of the AOAs towards chondrules, and provide possible mechanisms of transformation of refractory materials into chondrules or chondrule precursors. The rare occurrences of low-Ca pyroxene in AOAs may indicate that either AOAs were isolated from the hot nebular gas before condensation of low-Ca pyroxene or that condensation of low-Ca pyroxene by reaction between forsterite and gaseous SiO was kinetically inhibited. If the latter is correct, then the common occurrences of pyroxene-rich Type I chondrules may require either direct condensation of low-Ca pyroxenes or SiO_2 from fractionated nebular gas or condensation of gaseous SiO into chondrule melts. *Copyright © 2004 Elsevier Ltd*

1. INTRODUCTION

Amoeboid olivine aggregates (AOAs) are irregularly shaped objects consisting of forsteritic olivine ($Fa_{<2}$; in primitive chondrites only), FeNi-metal, and a refractory component [fine-grained minerals, either assembled into individual Ca,Al-rich inclusions (CAIs) or interspersed with forsterite grains] composed of Al-diopside, spinel, ±anorthite, and ±melilite. Originally defined in the oxidized CV chondrite Allende (Grossman and Steele, 1976), AOAs have been studied in most carbonaceous chondrite groups and several ungrouped carbonaceous chondrites, including reduced and oxidized CVs (McSween, 1977; Bar-Matthews et al., 1979; Cohen et al., 1983; Kornacki and Wood, 1984a,b; Hashimoto and Grossman, 1987; Komatsu et al., 2001; Imai and Yurimoto, 2003; Lin and Kimura, 2003; this study), COs (Rubin, 1998; Chizmadia et al., 2002; Itoh et al., 2002 this study), CMs (MacPherson et al., 1983; Hiyagon and Hashimoto, 1999; this study), CRs (Weisberg and Prinz, 1990; Weber and Bischoff, 1997; Aléon et al.,

* Author to whom correspondence should be addressed (sasha@higp.hawaii.edu).

2002; Weisberg et al., 2003; this study), CBs (Krot et al., 2001a), CH (Krot, unpubl.), Adelaide (Krot et al., 2001b; this study), Acfer 094 (Weber, 1995; Krot et al., 2003a,b,c; this study), and LEW85332 (Krot, unpublished data). AOAs are the least refractory objects genetically related to CAIs, and are chemically most similar to magnesian (Type I) chondrules, providing a possible genetic link between CAIs and chondrules.

Based on the mineralogy and petrology of AOAs in the reduced CV chondrites Efremovka and Vigarano, the thermodynamic considerations, the ^{16}O-rich compositions of AOAs, the depletion of AOAs in moderately volatile elements, such as Mn, Cr, and Na, and the absence of low-Ca pyroxene in AOAs, Komatsu et al. (2001) inferred that (i) AOAs are aggregates of gas-solid nebular condensates which experienced high-temperature annealing and solid-state recrystallization without substantial melting (see also Lin and Kimura, 1998). (ii) AOAs formed in CAI-forming region(s) and were largely absent from chondrule-forming region(s) at the time of chondrule formation. (iii) AOAs were either subsequently removed from this region before condensation of low-Ca pyroxene or gas-solid condensation of low-Ca-pyroxene was kinetically inhibited (Imae et al., 1993).

Here, we report the discovery of AOAs with low-Ca pyroxene and AOA/Al-rich chondrule-like objects in the CRs, CVs, CMs, Acfer 094, Adelaide, and LEW85332, and discuss their significance for understanding genetic relationship between the refractory inclusions and magnesian chondrules. We also carry out thermodynamic analysis of the high-temperature nebular reactions recorded by AOAs. Preliminary results of this work were reported in Krot et al. (2003a,b).

2. SAMPLES AND ANALYTICAL TECHNIQUES

Polished sections of the CR, CB, CH, CM, CV, CO, Acfer 094, Adelaide, and LEW85332 were X-ray mapped in Ca, Al, Mg, Si, Cr, Ni, Mn, Ti, and Na Kα with resolution of 5–10 μm (2 μm for individual AOAs) with a Cameca SX50 electron microprobe. The identified AOAs were studied in backscattered electron (BSE) mode with the scanning electron microscope JEOL 5900LV. Mineral compositions were determined with a Cameca SX50 electron microprobe using 15 keV accelerating voltage, 10–20 nA (for silicates) and 30 nA (for metal) current, a focused ($\sim$1–2 μm) beam, and well-characterized silicate, oxide and metal standards. For each element, counting times on both peak and background were 30 s (10 s for Na and K). Matrix corrections were applied using a PAP software routine. The element detection limits with the Cameca SX50 for silicates are (in wt%) SiO_2, Al_2O_3, MgO, 0.03; TiO_2, CaO, K_2O, 0.04; Na_2O, Cr_2O_3, 0.06; MnO, 0.07; FeO, 0.08.

3. RESULTS

3.1. AOAs in the Ungrouped Carbonaceous Chondrite Acfer 094

Acfer 094 is a unique, type 3 carbonaceous chondrite breccia with mineralogical, petrologic, nitrogen isotopic and oxygen isotopic affinities to the CM and CO groups (Newton et al., 1995; Greshake, 1997). Its O-isotopic composition and matrix modal abundance are similar to those of CO chondrites, whereas its bulk chemical composition is similar to that of CM chondrites. In contrast to CM chondrites, Acfer 094 shows no evidence for aqueous alteration and thermal metamorphism.

AOAs comprise $\sim$ 30% of all refractory inclusions in Acfer 094 (Krot et al., 2003c). These are irregularly shaped objects consisting of anhedral forsteritic olivine grains ($Fa_{<2}$), very minor FeNi-metal, and a refractory component (fine-grained minerals and individual CAIs) composed of anorthite, Al-diopside, spinel, and exceptionally rare melilite (Fig. 1). The olivine/CAIs ratios and modal mineralogy of the CAIs in AOAs vary in a broad range. Melilite, if present, is extensively

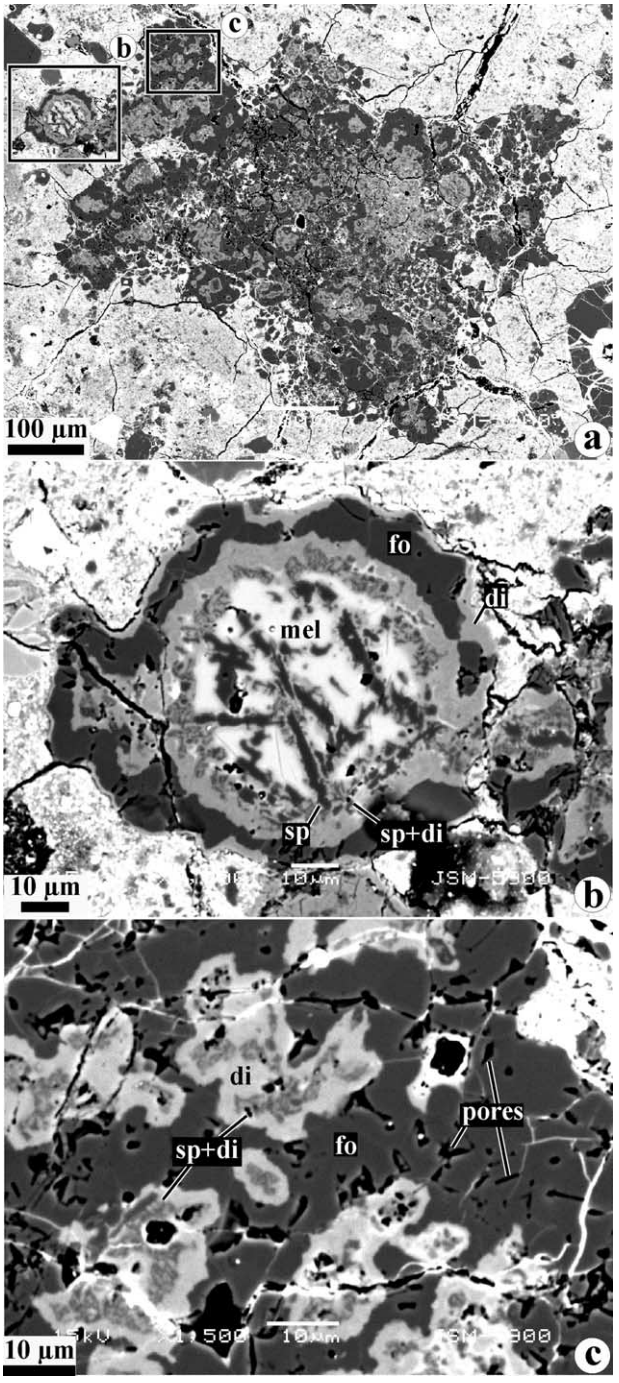

Fig. 1. BSE images of a melilite-bearing AOA in the ungrouped carbonaceous chondrite Acfer 094. The AOA consist of forsteritic olivine (fo) and CAIs composed of Al-diopside (di), spinel (sp), and melilite (mel). Melilite is replaced by a symplectitic intergrowth of spinel and Al-diopside. Regions outlined in (a) are shown in detail in (b) and (c).

Table 1. Mineralogy and petrology of AOAs with low-Ca pyroxene and AOA/Al-rich chondrule-like objects in carbonaceous chondrites.[a]

											Occurrences of low-Ca px			
Chondrite	Class.	Object	Size (μm)	fo	met	refr. (%)	Al-di	an	sp	mel	w/o FeNi ar.	FeNi	w/FeNi	Evid. melt.
						AOAs								
Acfer 094	Unique	105	220 × 300	+	+	~20	+	+	−	−	+			Yes
		115	300 × 300	+	+	~20	+	+	−	−	+			Yes
		213	150 × 350 fr	+	+	~60	+	+	+	+	+			Yes
		311	180 × 330 fr	+	+	<10	+	+	−	−	+			No
		321	235 × 470	+	+	<10	+	+	−	−		+		No
		338	280 × 300	+	+	<5	+	+	−	−		+		Yes
Adelaide	Unique	7	225 × 310	+	+	~40	+	+	+	−			+	Yes
		8	290 × 700 fr	+	+	<10	+	+	+	−			+	Yes
		34b	190 × 280	+	+	<10	+	+	−	−	+			No
		46	250 × 310	+	+	~20	+	+	+	−		+		Yes
Gao Guenie (b)	CR	4-1	400 × 670 fr	+	+	~50	+	+	+	−		+		No
		4-3	180 × 350 fr	+	+	<10	+	+	−	−		+		Yes
		4-6	150 × 300 fr	+	+	~40	+	+	+	−	+	+		No
		5-3	400 × 570 fr	+	+	~10	+	+	−	−	+			Yes
GRA95229	CR	17	200 × 530 fr	+	+	~20	+	+	−	−		+		No
NWA 1180	CR	5	180 × 240 fr	+	+	~15	+	+	−	−		+		Yes
		10	200 × 260	+	+	<10	+	+	−	−	+	+		No
PCA91082	CR	24	960 × 1280	+	+	>50	+	+	+	−	+			Yes
		35	950 × 1100	+	+	~25	+	+	+	−			+	Yes
QUE99177	CR	3	630 × 960	+	+	<5	+	+	−	−		+		No
Efremovka	CV	20	~1500	+	+	~50	+	+	+	−	+			No
Murchison	CM	32	85 × 140 fr	+	+	<10	+	+	−	−			+	Yes
LEW85332	unique	13	320 × 400 fr	+	+	<5	+	+	−	−		+		No
						AOA/Al-rich chondrule-like objects								
Leoville	CV	1	1500 × 3500	+	+	~30	+*	+	+	−	+			Yes
Adelaide	unique	47	80 × 230	+	+	~30	+*	+	+	−	+			Yes

[a] Al-di = Al-diopside; an = anorthite; fo = forsterite; mel = melilite; met = FeNi-metal; sp = spinel; fr = fragmented; refr = refractory component (in vol%); + = present; class. = classification; occurrences of low-Ca pyroxene: w/o FeNi = replacement of forsterite without association with FeNi metal; ar. FeNi = haloes around FeNi-metal nodules; w/FeNi = thick rims with abundant FeNi-metal; evid. melt. = petrographic evidence for melting. * augite.

replaced by a symplectitic intergrowth of spinel and Al-diopside (Figs. 1b,c) or by anorthite. No spinel grains were found in direct contact with forsterite; instead, they are surrounded by anorthite and/or Al-diopside, which are in corrosion relationship with spinel. Within an individual AOA, the aluminum content in diopside increases towards spinel or anorthite, indicative of diffusion-driven solid state reactions. FeNi-metal grains are minor or accessory, and preferentially enclosed by forsterite. Secondary minerals such as nepheline, sodalite, ferrous olivine, and phyllosilicates are absent.

Six out of 57 AOAs studied contain low-Ca pyroxene (Table 1); two of them are illustrated in Figure 2; others are shown in Figure EA1 (Electronic Annex, Elsevier Website, Science Direct). AOA #105 is a relatively compact, irregularly shaped object composed of forsterite ($Fa_{0.4}$), rare FeNi-metal grains, and numerous irregularly shaped Al-diopside-anorthite inclusions, which are uniformly distributed in the central part of the AOA and nearly absent in its periphery (Figs. 2a,b). The refractory inclusions lack clear mineralogical zoning, although Al-diopside tends to form a layer between anorthite and forsterite. FeNi-metal grains are preferentially enclosed by forsterite. Low-Ca pyroxene ($Fs_{0.6}Wo_{0.7}$) occurs as a 5–15 μm layer replacing forsterite in the outermost portion of the AOA (Fig. 2b). The similar textural occurrence of low-Ca pyroxene is found in AOA #311 having small abundance of Al-diopside-anorthite inclusions (Figs. AE1a,b).

AOA #213 is a fragmented object, ~150 × 350 μm in size, containing ~60 vol% of irregularly shaped CAIs and ~40 vol% of forsterite ($Fa_{0.5}$), low-Ca pyroxene ($Fs_{1.0}Wo_{0.6}$), and FeNi-metal grains (Figs. 2c–f). The CAIs consist of Al-diopside and tiny melilite grains, which are almost completely replaced by the symplectitic intergrowths of spinel and Al-diopside in the central part of the AOA and by anorthite in its outer part. FeNi-metal grains are uniformly distributed throughout the AOA; some of the metal grains occur inside the CAIs (Fig. 2e). Forsterite is extensively replaced by low-Ca pyroxene throughout the AOA (Figs. 2d–f). Abundant low-Ca pyroxene ($Fs_{0.9}Wo_{1.4}$) replacing forsterite ($Fa_{0.4}$) is also found in AOA #115 (Fig. AE1c,d).

AOA #321 consists of forsterite, numerous, irregularly shaped Al-diopside-spinel inclusions, and several FeNi-metal nodules, which are extensively weathered. Low-Ca pyroxene ($Fs_{0.6}Wo_{1.8}$) replaces forsterite ($Fa_{0.2}$) around FeNi-metal nodules (Figs. AE1e,f). The similar textural occurrence of low-Ca pyroxene was found in AOA #338.

Forsterite grains in AOAs with low-Ca pyroxene (px-AOAs) show smaller range in MnO contents than those in AOAs without low-Ca pyroxene (Table AE1; Fig. AE2). There are no significant compositional differences between Al-diopsides in px-AOAs and AOAs without low-Ca pyroxene (Table AE2; Fig. AE3). Low-Ca pyroxenes have low MnO and Cr_2O_3, which, however, are significantly higher than those in Al-

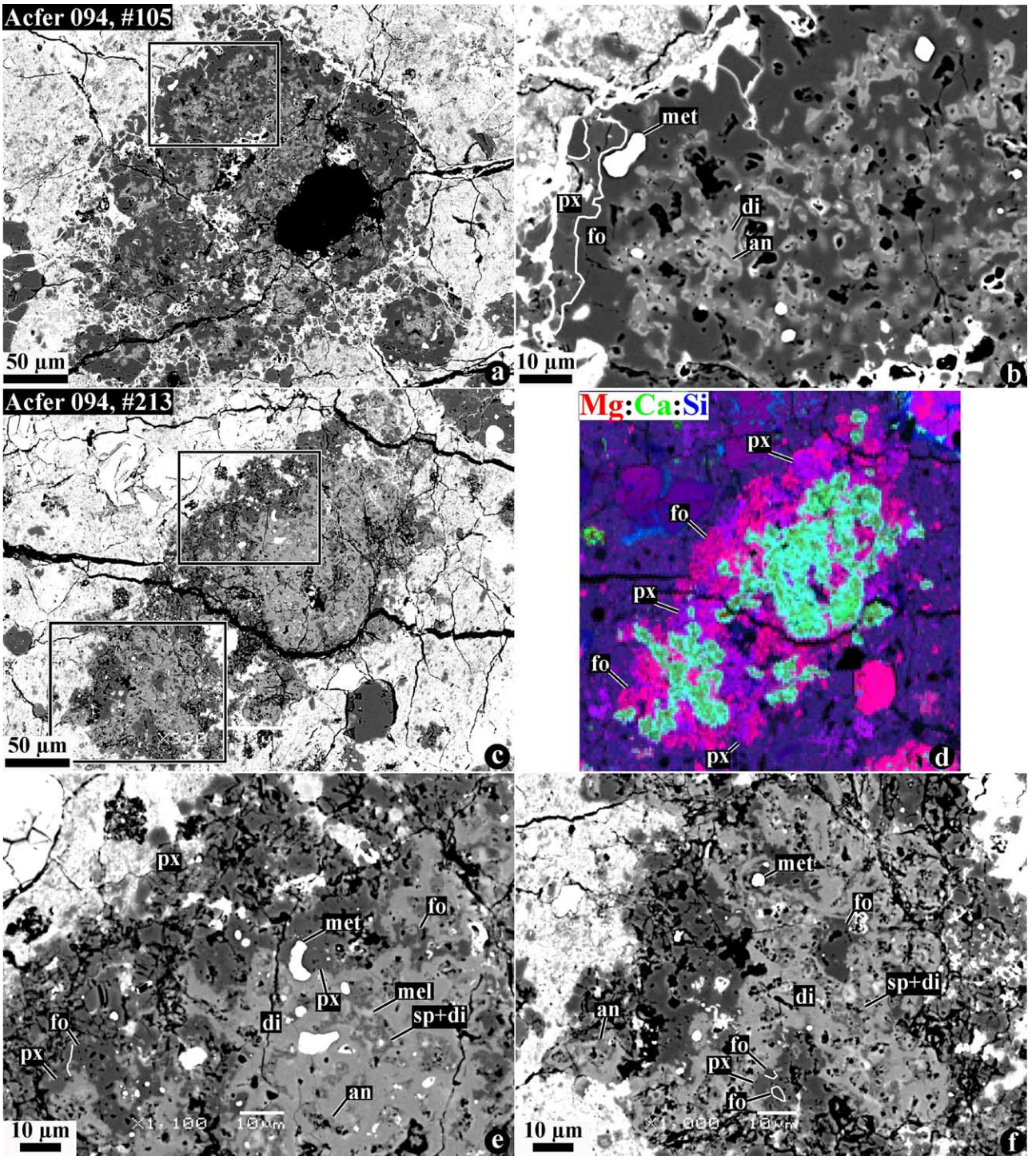

Fig. 2. BSE images (a-c, e, f) and a combined X-ray elemental map (d) in Mg (red), Ca (green), and Si Kα (blue) of AOAs with low-Ca pyroxene in Acfer 094. (a, b) AOA #105 consists of forsterite, rare FeNi-metal grains (met), and numerous irregularly shaped Al-diopside-anorthite inclusions, which are uniformly distributed in the central part of the AOA and nearly absent in its outer part. FeNi-metal grains are preferentially concentrated in forsterite. Low-Ca pyroxene (px; outlined in (b)) replaces forsterite in the outermost portion of the AOA. Region outlined in (a) is shown in detail in (b). (c–f) AOA #213 contains ~60 vol% of irregularly shaped CAIs and ~40 vol% of forsterite, low-Ca pyroxene, and FeNi-metal grains. The CAIs consist of Al-diopside and melilite, which is almost completely replaced by a symplectitic intergrowth of spinel and Al-diopside in the central part of the AOA and by anorthite in its outer part. Forsterite is extensively replaced by low-Ca pyroxene (forsterite is slightly darker than low-Ca pyroxene in BSE images; in color map, low-Ca pyroxene is bluish, whereas forsterite is reddish); relict regions of forsterite in low-Ca pyroxene are outlined in (f). FeNi-metal grains are uniformly distributed throughout the AOA and found in both CAIs and ferromagnesian silicates. Regions outlined in (c) are shown in detail in (e) and (f).

Table 2. Representative electron microprobe analyses of low-Ca and sub-Ca pyroxenes in AOAs and AOA-like objects in carbonaceous chondrites.[a]

Chondrite	Acfer 094						Adelaide			PCA91082		Gao	NWA	Efr	Mrch	Leoville	
AOA #	105	115	213	311	321	338	7	46	47*	35	24	4–6	10	20	32	1*	1*
SiO_2	55.9	56.6	57.9	58.6	58.6	51.5	58.5	57.5	56.5	57.5	59.4	57.0	58.11	58.2	56.7	57.3	55.6
TiO_2	0.22	0.30	<0.09	0.34	0.19	0.22	0.30	0.39	1.6	0.17	<0.09	<0.09	0.27	0.28	0.52	0.66	0.67
Al_2O_3	0.25	0.39	0.21	0.52	0.53	1.2	0.85	1.1	2.2	2.0	0.58	0.27	0.38	0.37	1.1	1.6	1.7
Cr_2O_3	0.30	0.40	0.33	0.35	0.27	0.47	0.75	1.0	0.69	0.84	0.27	0.28	0.19	0.18	0.67	0.56	0.62
FeO	0.78	0.63	0.74	0.69	0.46	2.7	1.5	3.0	0.86	1.8	0.81	2.0	1.0	1.3	1.6	0.57	0.96
MnO	0.06	0.12	0.12	0.12	0.08	0.26	0.32	0.48	0.20	0.37	0.09	0.10	<0.07	0.08	0.29	0.07	0.12
MgO	38.7	38.8	39.8	38.4	39.2	41.5	36.2	34.8	36.1	35.6	39.6	38.7	39.7	38.4	38.3	38.4	32.2
CaO	0.74	0.77	0.26	1.5	0.98	1.3	1.9	2.9	2.7	2.6	0.60	0.37	0.82	0.75	2.4	0.76	7.4
Na_2O	<0.06	<0.06	<0.06	<0.06	<0.06	<0.06	<0.06	<0.06	<0.06	<0.06	<0.06	<0.06	<0.06	<0.06	<0.06	<0.06	<0.06
K_2O	<0.04	<0.04	<0.04	<0.04	<0.04	<0.04	<0.04	<0.04	<0.04	<0.04	<0.04	<0.04	<0.04	<0.04	<0.04	<0.04	<0.04
total	96.9	98.1	99.4	100.5	100.3	99.2	100.3	101.2	100.9	100.9	101.4	98.7	100.6	99.6	101.5	99.9	99.3
Fs	1.1	0.9	1.0	1.0	0.6	3.4	2.1	4.4	1.3	2.7	1.1	2.8	1.4	1.9	2.2	0.8	1.4
Wo	1.3	1.4	0.5	2.7	1.8	2.2	3.6	5.4	5.1	4.9	1.1	0.7	1.4	1.4	4.2	1.4	13.9

[a] NWA = NWA 1180; Efr = Efremovka; Mrch = Murchison; * AOA/chondrule-like objects.

diopside (Table 2; Fig. AE3). Spinel and anorthite in px-AOAs are too fine-grained for microprobe analyses. Due to small grain sizes and terrestrial weathering, only few FeNi-metal grains were analyzed in px-AOAs. Two metal grains in AOA #105 are compositionally similar (Ni, 5.5–6.5 wt%; Co, 0.35–0.42 wt%), whereas those in AOA #213 are significantly different in composition (Ni, 5.5 and 12.3 wt%; Co, 0.42–0.47 wt%).

3.2. AOAs in the Ungrouped Carbonaceous Chondrite Adelaide

Adelaide is an anomalous carbonaceous chondrite with the affinities to the CM-CO clan (Fitzgerald and Jones, 1977; Davy et al., 1978; Hutcheon and Steele, 1982; Kallemeyn and Wasson, 1982; Kerridge, 1985; Huss and Hutcheon, 1992), which, however, escaped thermal metamorphism and alteration commonly observed in the CM and CO chondrites.

AOAs comprise ~30% of all refractory inclusions identified in Adelaide (Krot et al., 2001b), and are irregularly shaped or rounded objects consisting of anhedral forsterite, weathered FeNi-metal nodules, and a refractory component (fine-grained minerals and individual CAIs) composed of anorthite, Al-diopside, and spinel; no melilite was found. The olivine/CAIs ratios and modal mineralogy of the CAIs in AOAs vary in a wide range. Spinel grains are typically surrounded by anorthite or by a mixture of anorthite and Al-diopside, and are replaced by these minerals to a various degree (Fig. 3). Secondary nepheline, sodalite, ferrous olivine, and phyllosilicates are absent.

Four out of ~ 50 AOAs studied contain low-Ca pyroxene (Fig. 4). AOA #8 is an irregularly shaped, fragmented object, ~290 × 700 μm in size, containing ~80 vol% of a refractory component and ~20 vol% of ferromagnesian silicates (Figs. 4a,b). The refractory component consists of Al-diopside and coarse spinel grains that are replaced by Al-diopside and anorthite. The Al-content in diopside increases towards spinel and anorthite. The AOA is surrounded by a discontinuous layer of low-Ca pyroxene (identified using EDS and X-ray mapping) with abundant inclusions of FeNi-metal. Low-Ca pyroxene corrodes and contains relict inclusions of forsterite ($Fa_{1.4}$).

AOA #7 is a compact object, ~225 × 310 μm in size, composed of forsterite ($Fa_{0.3}$), FeNi-metal nodules, coarse-grained spinel corroded by anorthite, and Al-diopside (Fig. 4c). Metal is preferentially concentrated in forsterite. The AOA is surrounded by a continuous shell of low-Ca pyroxene ($Fs_{2.1}Wo_{3.6}$) with abundant tiny inclusions of FeNi-metal; low-Ca pyroxene replaces forsterite.

AOA #34b (Fig. 4d) contains ~10 vol% of very fine-grained anorthite and Al-diopside surrounded by porous and compact forsterite ($Fa_{0.4}$), which is replaced by low-Ca pyroxene (identified using EDS and X-ray mapping).

AOA #46 is an ellipsoidal, compact object, ~250 × 310 μm in size, composed of forsteritic olivine ($Fa_{3.6}$), abundant FeNi-metal nodules, and numerous irregularly shaped Al-diopside-anorthite±spinel inclusions. The AOA is surrounded by a thin (<4 μm), continuous layer of low-Ca pyroxene ($Fs_{4.4}Wo_{5.4}$) without visible inclusions of FeNi-metal.

Olivine grains in the Adelaide AOAs without low-Ca pyroxene are nearly pure forsterite ($Fa_{<1}$), poor in Cr_2O_3 (<0.3 wt%), and generally MnO-free (<0.07 wt%), whereas those in px-AOAs tend to have higher Cr_2O_3 (0.2–0.6 wt%), MnO (up to 0.8 wt%), and fayalite content (1–4 mol%) (Table AE1; Fig. AE4). Spinel grains are FeO-poor [Mg/(Mg + Fe) > 0.98] and contain <0.45 wt% Cr_2O_3 (Table AE3). Plagioclase is end-member anorthite (Table AE4). Diopside shows large variations in Al_2O_3 (0.5–16 wt%) and TiO_2 (0.1–7 wt%) (Table AE2; Fig. AE5). Most diopsides are MnO-free (<0.07 wt%) and Cr_2O_3-poor (<0.2 wt%). Low-Ca pyroxenes have relatively high Cr_2O_3 (0.6–1.1 wt%), moderately high MnO (0.3–0.5 wt%), and low TiO_2 (0.2–0.4 wt%) (Table 2; Fig. AE5).

3.3. AOAs with Low-Ca Pyroxene in the Ungrouped Carbonaceous Chondrite LEW85332

The only px-AOA (#13) found in LEW85532 consists mainly of forsteritic olivine ($Fa_{1.7}$, 0.13 wt% Al_2O_3, 0.54 wt% Cr_2O_3, 0.39 wt% MnO) and FeNi-metal nodules. Low-Ca pyroxene ($Fs_{1.5}Wo_{2.8}$, 0.25 wt% TiO_2, 0.7 wt% Cr_2O_3, 0.72 wt% Al_2O_3, 0.2 wt% MnO) forms haloes around FeNi-metal (Fig. AE6).

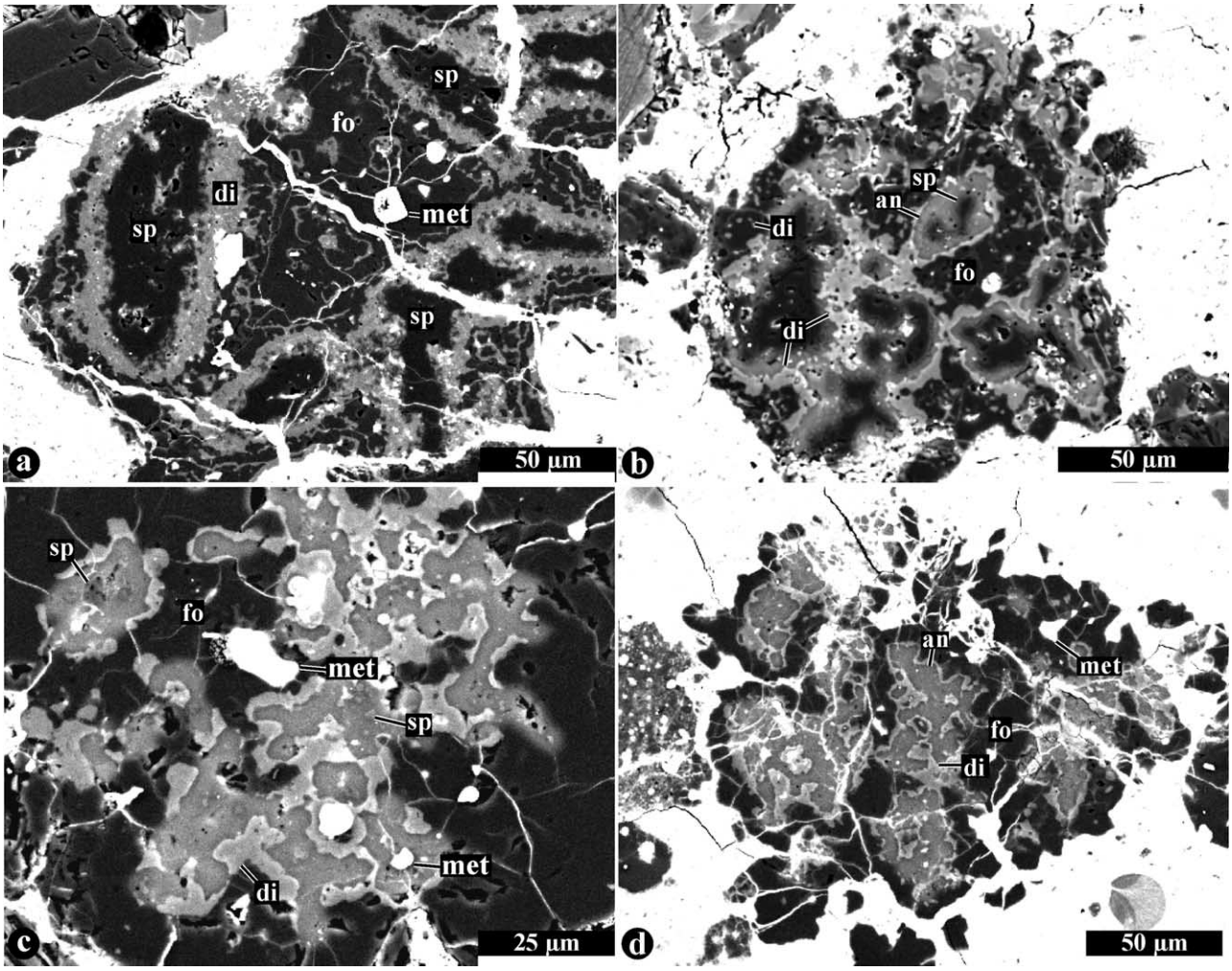

Fig. 3. BSE images of AOAs without low-Ca pyroxene in the ungrouped carbonaceous chondrite Adelaide. AOAs consist of forsterite, FeNi-metal grains, and a refractory component composed of Al-diopside, anorthite, and spinel. The olivine/CAIs ratios and modal mineralogy of the CAIs in AOAs vary in a broad range. Spinel is replaced by Al-diopside and/or anorthite to a various degree.

3.4. AOAs with Low-Ca Pyroxene in CR Chondrites

The mineralogy and petrology of AOAs in CR chondrites have been recently characterized by Aléon et al. (2002) and by Weisberg et al. (2003); no px-AOAs have been reported. We find that ~10% of AOAs in CRs contain low-Ca pyroxene (Table 1). AOAs with different textural occurrences of low-Ca pyroxene are described below.

AOA #35 in PCA91082 is an irregularly shaped object, ~950 × 1100 μm in size, consisting of Cr-bearing forsterite (Fa_1; Cr_2O_3, 0.84 wt%), abundant FeNi-metal nodules, and numerous irregularly shaped Al-diopside-anorthite inclusions; some of the inclusions contain minor spinel (Fig. 5). The AOA is mineralogically zoned: its core is FeNi-metal-poor and contains most of the CAIs; mantle zone contains abundant FeNi-metal nodules and only a few CAIs. The outermost portion of the AOA consists of low-Ca pyroxenes (Fs_3Wo_5) with abundant, tiny inclusions of FeNi-metal (Fig. 5d).

AOA #24 in PCA91082 is an irregularly shaped object, ~960 × 1280 μm in size, containing ~50 vol% of CAIs surrounded by a relatively porous aggregate of forsterite grains; both components contain rounded inclusions of FeNi-metal (Fig. 6). The CAIs consist of diopside, tiny anhedral spinel intergrown with Al-rich diopside, and rare melilite ($Åk_{13}$), which occurs only in central region of the AOA. Low-Ca pyroxene ($Fs_{1.6}Wo_{0.9}$) occurs as anhedral grains replacing forsterite ($Fa_{0.5}$) along grain boundaries and around FeNi-metal nodules; it also forms subhedral grains around large FeNi-metal nodule (Fig. 6c). The similar textural occurrences of low-Ca pyroxene are found in the Gao-Guenie (b) AOAs #5–3, 4–1, 4–3, and 4–6, NWA 1180 (Figs. 7a,b), QUE99177 AOA #3 (Fig. 7c), and GRA95229 AOA #17 (Fig. 7d). Among these AOAs, the NWA AOA #10 has the highest porosity and the highest abundance of low-Ca pyroxene.

AOA #5 in NWA 1180 (Figs. 7e,f) is a compact object that contains subhedral and euhedral grains of Al-diopside in anorthite, suggesting that it experienced melting. This is consistent with the presence of rounded metal nodules throughout the AOA components. Low-Ca pyroxene (identified qualitatively

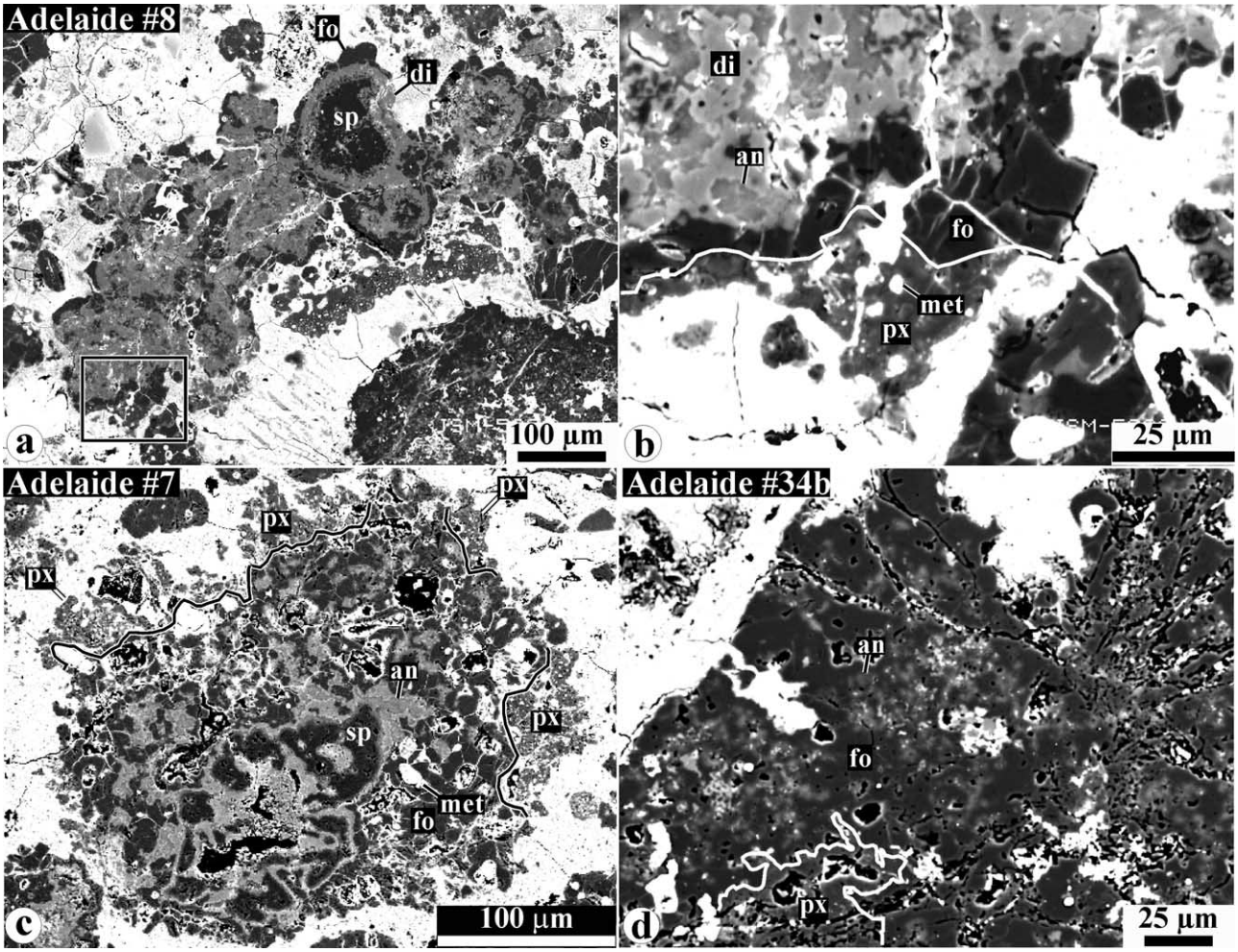

Fig. 4. BSE images of AOAs with low-Ca pyroxene in Adelaide. (a, b) AOA #8 is dominated by a refractory component composed of Al-diopside, spinel, and minor anorthite. Coarse spinel grains are corroded by Al-diopside and anorthite. The refractory component is surrounded by the fragmented layers of forsterite and low-Ca pyroxene. The low-Ca pyroxene layer is in corrosion relationship with the forsterite layer and contains abundant opaque inclusions (weathered FeNi-metal) and rare relict regions of forsterite. Regions outlined in (a) is shown in detail in (b). (c) AOA #7 consists of forsterite, spinel, anorthite, Al-diopside, and FeNi-metal. The spinel grains are anhedral and are corroded by anorthite that is separated from forsterite by a layer of Al-diopside. AOA is surrounded by a continuous layer, up to 50 μm in thickness, of low-Ca pyroxene (outlined in (c)) with abundant, tiny inclusions of FeNi-metal; low-Ca pyroxene replaces forsterite. (d) AOA #34b consists of porous forsterite regions with very fine-grained anorthite and Al-diopside; these regions are surrounded by compact forsterite rims. Both occurrences of forsterite are replaced by low-Ca pyroxene (outlined in (d)).

using EDS) is minor and replaces forsterite ($Fa_{1.3}$) in the outer portion of the AOA.

There are no compositional differences in olivine in the CR AOAs with and without low-Ca pyroxenes (Table AE1; Fig. AE7). Similar to px-AOAs in Acfer 094 and Adelaide, low-Ca pyroxene in the CR AOAs contains higher Cr_2O_3 and MnO contents than Al-diopside (Table 1; Fig. AE8).

3.5. AOA with Low-Ca Pyroxene in the Reduced CV Chondrite Efremovka

The mineralogy and petrology of AOAs from the reduced CV chondrites have been recently characterized by Komatsu et al. (2001). Here, we describe the only AOA with low-Ca pyroxene (#20) found in Efremovka. This irregularly shaped AOA (Figs. 8a,b), ~1.5 mm in apparent diameter, contains ~70 vol% of CAIs composed of fine-grained spinel, anorthite, and Al-diopside, and ~30 vol% of forsterite ($Fa_{0.8}$; Table AE1). Spinel occurs as anhedral grains completely surrounded for anorthite. Al-diopside is closely intergrown with forsterite and typically separates anorthite from forsterite; it also forms tiny inclusions in forsterite. Forsterite grains in the outermost portion of the AOA are replaced by low-Ca pyroxene ($Fs_{1.9}Wo_{1.4}$; Table 1).

3.6. AOA with Low-Ca Pyroxene in the CM Chondrite Murchison

AOAs are the dominant type of refractory inclusions in Murchison (e.g., MacPherson et al., 1983). They consist of

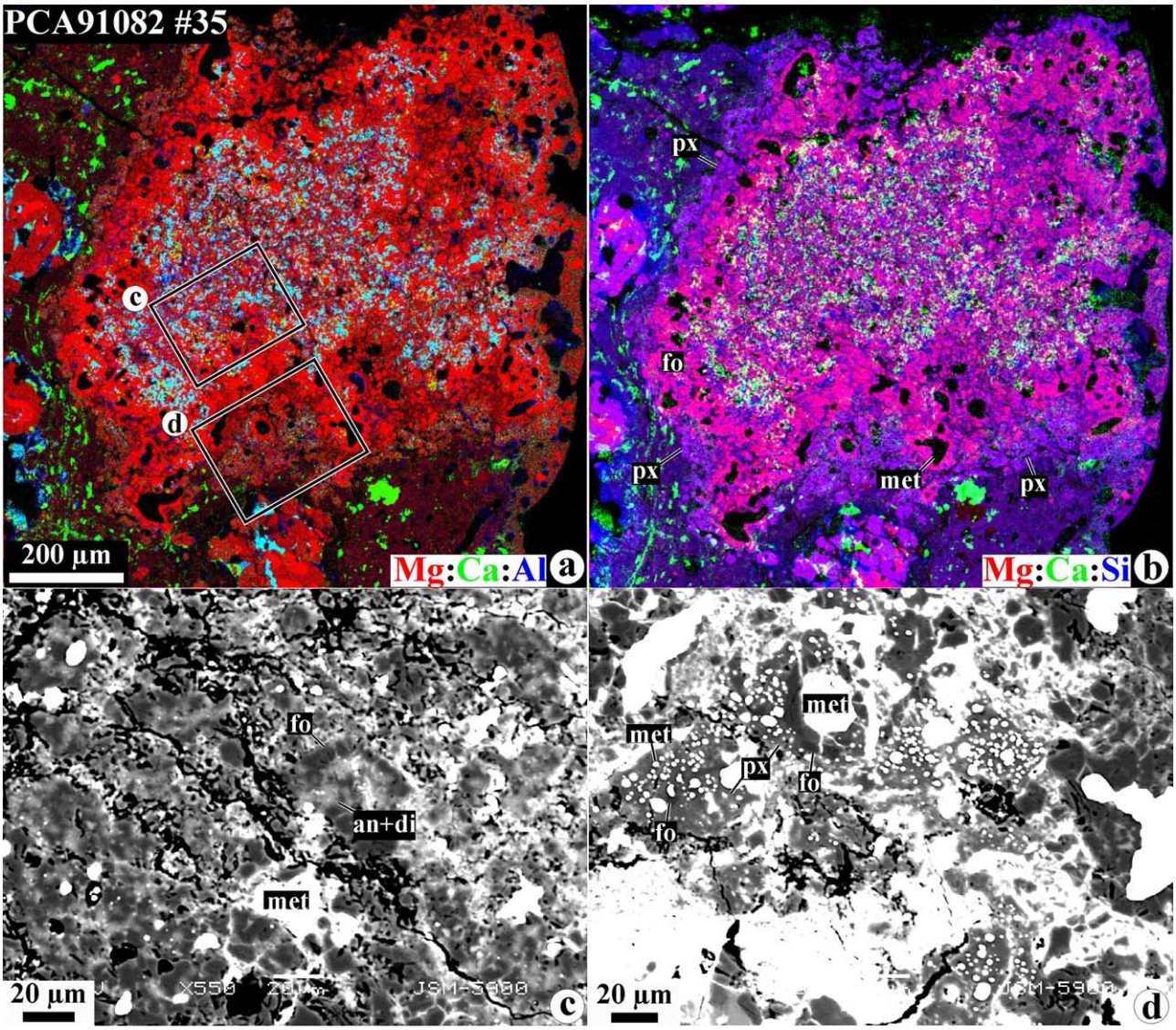

Fig. 5. Combined X-ray elemental maps in Mg (red), Ca (green), and Al Kα (blue) (a), and Mg (red), Ca (green), and Si Kα (blue) (b), and BSE images (c, d) of AOA #35 with low-Ca-pyroxene in the CR carbonaceous chondrite PCA91082. The AOA consists of forsterite, anorthite, Al-diopside, and FeNi-metal, and is mineralogically zoned. Its core is enriched in Al-diopside and anorthite and depleted in FeNi-metal relative to the mantle zone. AOA is surrounded by a continuous layer of low-Ca pyroxene (bluish in (b)) with abundant, tiny inclusions of FeNi-metal. The pyroxene replaces forsterite. Regions outlined in (a) are shown in detail in (c, d).

forsterite and a refractory component composed of Al-diopside, spinel, and exceptionally rare anorthite; no FeNi-metal grains were found. The refractory component is either extensively replaced by phyllosilicates or nearly completely leached out; the latter process results in large porosity of AOAs. In contrast, the only AOA with low-Ca pyroxene found in Murchison (#32) is a compact object, ~85 × 140 μm in size, that shows little evidence for alteration of the refractory component (Figs. 8c,d). It consists of forsterite ($Fa_{1.1}$; Table AE1) enclosing rare opaque nodules and abundant irregularly shaped regions composed of anorthite with euhedral and subhedral inclusions of Al-diopside. The similar textural appearance of Al-diopside was described in the NWA 1180 AOA #5 (Figs. 7e,f) and probably suggests crystallization from melt. Forsterite in the outermost portion of the AOA is replaced by Al-bearing low-Ca pyroxene (Fs_2Wo_4, ~1 wt% Al_2O_3; Table 2) containing tiny inclusions of magnetite and sulfides (Fig. 8d).

3.7. AOA/Al-Rich Chondrule-Like Objects in the Reduced CV Chondrite Leoville and Ungrouped Carbonaceous Chondrite Adelaide

In this section, we describe two forsterite-rich objects with high abundance of anorthite, spinel and high-Ca Al-rich pyroxenes, which may represent extensively melted AOAs.

Leoville #1 (L1; Fig. 9) is an irregularly shaped object, ~1.5 × 3.5 mm in size, composed of subhedral and euhedral forsterite

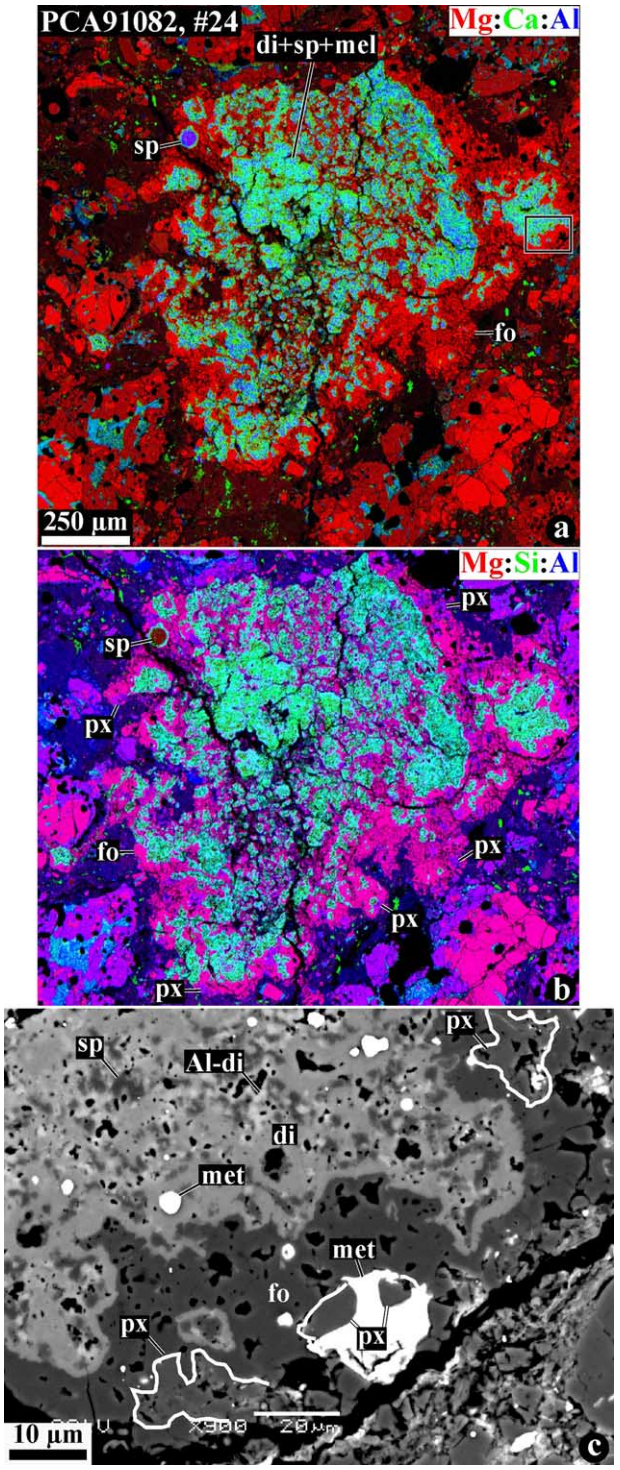

Fig. 6. Combined X-ray elemental maps in Mg (red), Ca (green), and Al Kα (blue) (a), and Mg (red), Ca (green), and Si Kα (blue) (b) and BSE image (c) of AOA #24 in PCA91082. The AOA contains ~50 vol% of CAIs surrounded by a relatively porous aggregate of forsterite grains; both components contain rounded inclusions of FeNi-metal. The CAIs consist of Al-diopside, spinel, and minor anorthite and melilite. Low-Ca pyroxene (outlined in (c)) replaces forsterite along grain boundaries and around FeNi-metal nodules; it also forms subhedral grains around large FeNi-metal nodule. Region outlined in (a) is shown in detail in (c).

grains ($Fa_{0.9-2.4}$; Table AE1), spinel (Table AE3) anorthitic plagioclase or mesostasis ($An_{95.9\pm2.7}$; Table AE4), and igneously zoned pyroxenes ranging in compositions from low-Ca pyroxene (Fs_1Wo_1) to pigeonite (Fs_1Wo_5) to high-Ca pyroxene (Fs_1Wo_{40}) (Tables 2 and AE2). Spinel occurs as clusters of small grains surrounded by anorthitic plagioclase (Figs. 9d,f). Forsterite shows large variations in grain size (Fig. 9e) and often forms chains of grains surrounding spinel-anorthite regions (Fig. 9f). X-ray mapping of L1 revealed its complex mineralogical zoning (Fig. 9a–c). Core of L1 is metal-free and contains abundant Ca,Al-rich minerals; it is surrounded by a forsterite-rich zone that is poor in Ca,Al-rich minerals. Ca,Al-rich minerals are heterogeneously distributed in the core (Fig. 9a). Its left portion contains several relatively coarse-grained spinel-anorthite-rich regions surrounded by fine-grained material composed of closely intergrown forsterite, pigeonite and high-Ca pyroxene (Fig. 9d). The right portion of the core has less spinel and coarser grains of forsterite, pigeonite, augite, and plagioclase (Fig. 9e). Forsterite in the peripheral zone is replaced by low-Ca pyroxene (Fig. 9f). L1 is surrounded by a discontinuous layer largely composed of low-Ca pyroxene and FeNi-metal nodules (Fig. 9c).

Adelaide #47 (Fig. 10) is an irregularly shaped object, ~80 × 230 μm in size, that contains several regions of small spinel grains surrounded by anorthitic plagioclase or mesostasis (An_{98}; Table AE4) and subhedral forsterite grains ($Fa_{0.9}$; Table AE1). Forsterite grains in the outermost portion of the object are replaced by pigeonitic pyroxene ($Fs_{1.3}Wo_{5.1}$; Table 2). Small grains of pigeonitic pyroxene overgrown by augite occur also in plagioclase.

3.8. Summary of Mineralogical and Petrographic Observations of AOAs in Carbonaceous Chondrites

AOAs in primitive (unmetamorphosed) carbonaceous chondrites consist of forsterite, FeNi-metal, and a refractory component (fine-grained minerals or individual CAIs) composed of Al-diopside, spinel, anorthite, and melilite. Secondary minerals, such as nepheline, sodalite, ferrous olivine, and Ca,Fe-rich pyroxenes, commonly observed in the oxidized CV chondrites and metamorphosed CO chondrites, are absent. The refractory inclusions in AOAs are typically mineralogically zoned: their central zone consists of spinel grains and/or melilite, which is very rare. Melilite is extensively replaced by a symplectitic intergrowth of spinel and Al-diopside. The spinel core (if present) is surrounded by Al-diopside, with Al content increasing towards spinel, or by a fine-grained symplectitic intergrowth of spinel and Al-diopside followed by a monomineralic layer of Al-diopside, or by anorthite ±monomineralic layer of Al-diopside, with Al content increasing towards anorthite. There are corrosion relationships between spinel and the surrounding Al-diopside and/or anorthite. FeNi-metal grains are generally enclosed by forsterite.

Low-Ca pyroxene occurs in the outermost portion of ~ 5–10% of AOAs (due to extensive fragmentation of AOAs, this is probably a lower limit); it replaces forsterite and often contains relict forsterite grains. There are large variations in the degree of forsterite replacement, from very minor (<2 vol%; Fig. 2b) to extensive (~50 vol%; Figs. 2c–f). There are several textural occurrences of low-Ca pyroxene in AOAs: (i) thin (<10 μm) discontinuous layers

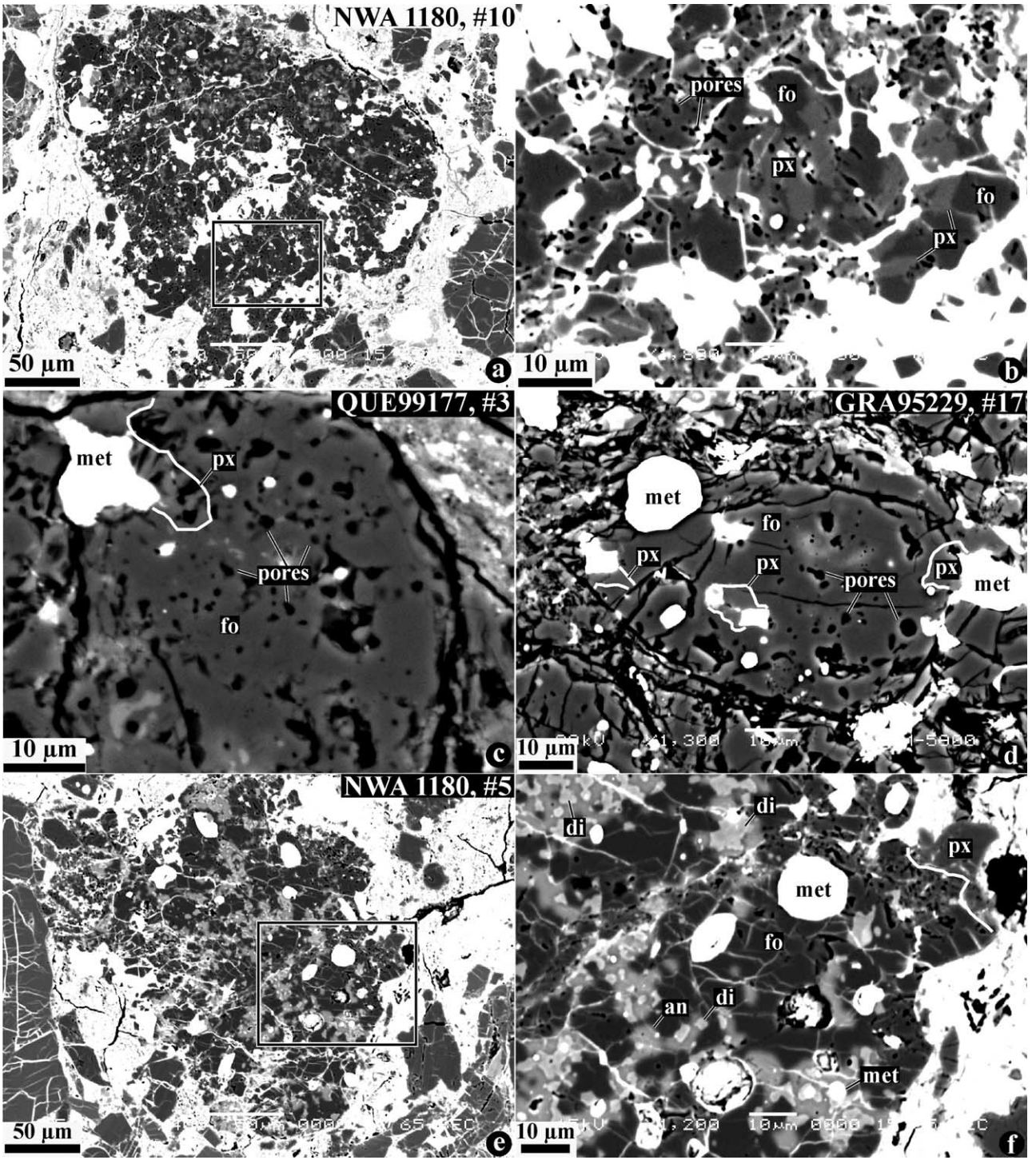

Fig. 7. BSE images of AOA #10 (a, b), #3 (c), #17 (d) and #5 (e, f) in the CR chondrites NWA 1180, QUE99177, and GRA95229. The AOA #10 (a, b) is an irregularly shaped, porous aggregate of forsterite, numerous irregularly shaped inclusions composed of anorthite and minor Al-diopside, and FeNi-metal grains preferentially concentrated in forsterite. Low-Ca pyroxene replaces forsterite along grain boundaries and around FeNi-metal nodules in the peripheral portion of the AOA. Region outlined in (a) is shown in detail in (b). The AOAs #3 (c) and #17 (d) are porous objects with low-Ca pyroxene (outlined in (c) and (d)) occurring around FeNi-metal nodules. The AOA #5 (e, f) is composed of forsterite, FeNi-metal, Al-diopside and anorthite, has a compact texture. Al-diopside occurs as subhedral and euhedral grains in anorthite probably indicating crystallization from melt. FeNi-metal nodules are preferentially concentrated in forsterite. Low-Ca pyroxene (outlined in (f)) occurs in the outermost portion of the AOA and corrodes forsterite. Region outlined in (e) is shown in detail in (f).

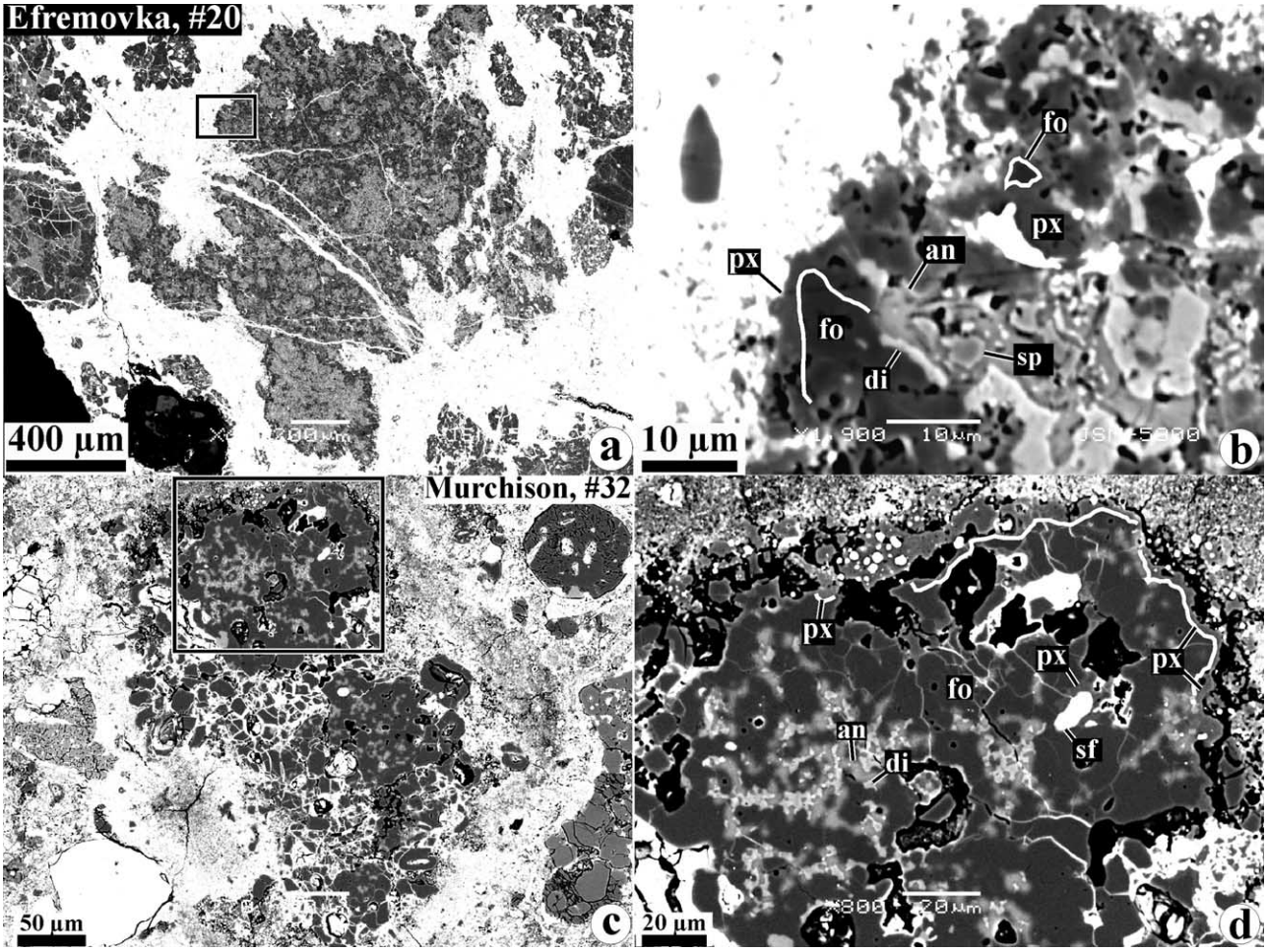

Fig. 8. BSE images of the AOAs with low-Ca pyroxene #20 in the reduced CV chondrite Efremovka (a, b), and #32 (c, d) in the CM chondrite Murchison. The AOA #20 (a, b) consists of anorthite, Al-diopside, spinel, forsterite, and low-Ca pyroxene. Spinel grains are anhedral and are corroded by anorthite that is typically separated from forsterite by a layer of Al-diopside. Low-Ca pyroxene (outlined in (b)) occurs in the outermost portion of the AOA and replaces forsterite; relict regions of forsterite occur in low-Ca pyroxene. The AOA #32 (c, d) consists of forsterite, anorthite, Al-diopside, FeNi-sulfides (sf) and low-Ca pyroxene. Al-diopside occurs as subhedral grains in anorthite, suggesting crystallization from melt. Sulfide nodules are preferentially concentrated in forsterite. Forsterite in the outermost portion of the AOA is replaced by low-Ca pyroxene (outlined in (d)) containing abundant, heterogeneously distributed inclusions of FeNi-sulfides. Regions outlined in (a) and (c) are shown in detail in (b) and (d), respectively.

around forsterite grains in AOA peripheries (e.g., Figs. 2b, 8b); (ii) veinlets along forsterite grain boundaries, which are largely concentrated in AOA peripheries (e.g., Figs. 6c, 7b); (iii) haloes and subhedral grains around FeNi-metal grains, which are largely concentrated in AOA peripheries (e.g., Figs. 6c, 7c,d), and (iv) thick (up to 70 μm) continuous layers with abundant tiny inclusions of FeNi-metal grains around AOAs (e.g., Figs. 4a–c, 5d, 8d). The first three occurrences of low-Ca pyroxene are commonly observed within an individual AOA.

Although AOAs with low-Ca pyroxene are mineralogically similar to those without low-Ca pyroxene, the former appear to be more compact and show evidence for melting of a small degree (Table 1). These include the presence of euhedral or subhedral grains of Al-diopside in anorthite (Figs. 7f, 8d) and the presence of euhedral grains of forsterite overgrown by diopside. The melting is also consistent with the presence of rounded FeNi-metal nodules throughout the AOAs (Figs. 2f, 6c). Low-Ca pyroxene shells with abundant tiny FeNi-metal nodules may have also experienced melting (Figs. 4b,c, 5d, 8d).

4. DISCUSSION

4.1. AOAs as Aggregates of Solar Nebula Condensates

Most AOAs are irregularly shaped objects consisting of three major components: Ca,Al-rich component composed of Al-diopside, anorthite, spinel, and melilite, ferromagnesian component composed of forsterite and low-Ca pyroxene, and FeNi-metal. There are significant variations in modal abundances of these components. Although AOAs show no evidence for being extensively melted, some CAIs in AOAs are rounded, compact objects, which probably experienced crystallization from melts.

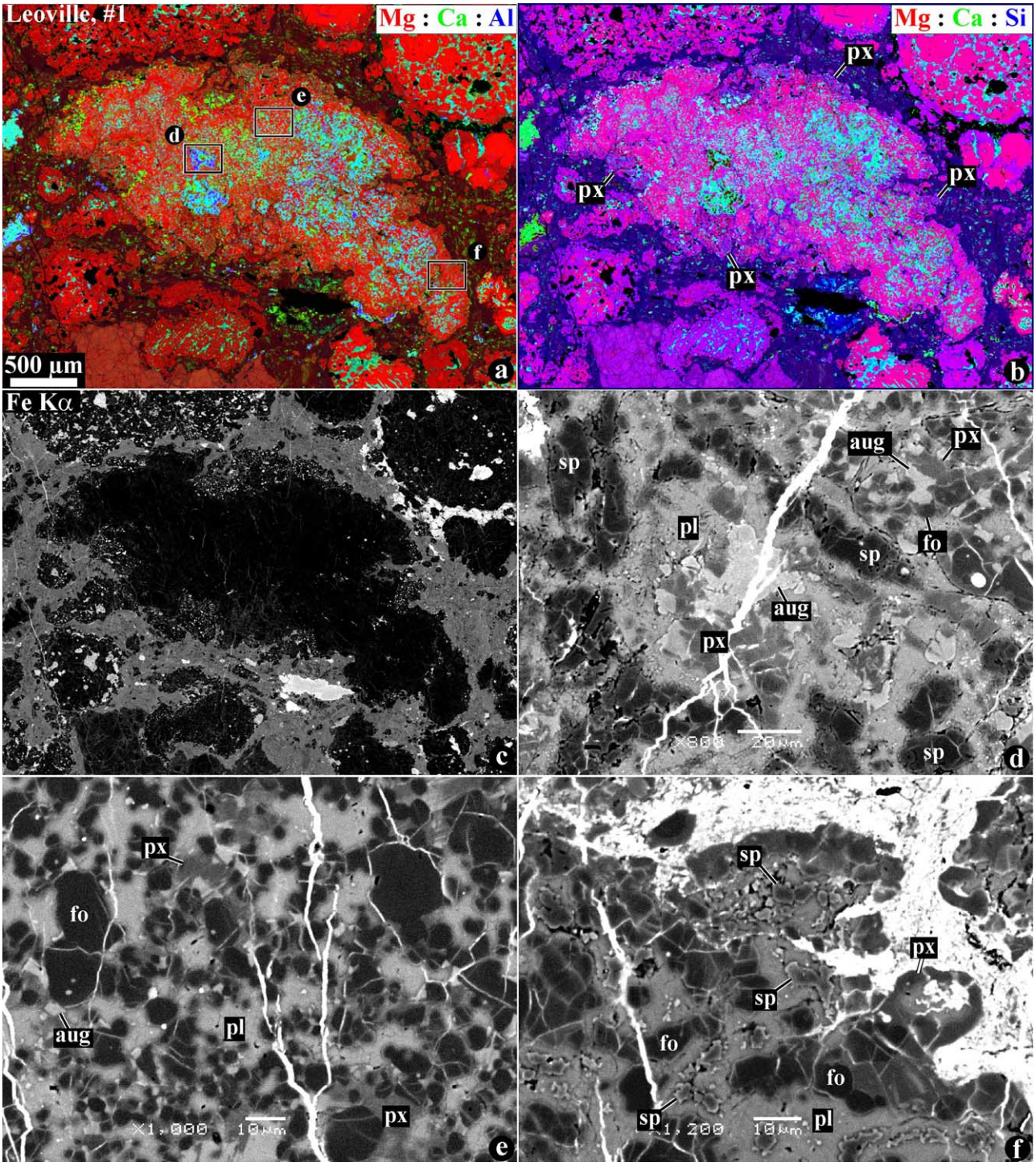

Fig. 9. Combined X-ray elemental maps in Mg (red), Ca (green), and Al Kα (blue) (a), and Mg (red), Ca (green), and Si Kα (blue) (b), elemental map in Fe Kα (c) X-rays, and BSE images (d–f) of AOA/Al-rich chondrule-like object #1 (L1) in the reduced CV chondrite Leoville. The L1 shows a complex mineralogical zoning: central zone is metal/sulfide-free and contains abundant Ca, Al-rich minerals, whereas outer zone is poor in Ca, Al-rich minerals and contains abundant FeNi-metal-sulfide grains. Ca, Al-rich minerals are also heterogeneously distributed in the central zone: its left portion (d) contains coarse-grained spinel-anorthite-rich regions surrounded by fine-grained material composed of closely intergrown forsterite, pigeonite (px) and augite (aug). The right portion (e) contains less spinel and coarser grains of forsterite, pigeonite, augite and plagioclase. Forsterite in the outermost portion of L1 is replaced by low-Ca pyroxene (f). The outer zone is composed of low-Ca pyroxene with abundant FeNi-metal nodules. Regions outlined in (a) are shown in detail in (d–f).

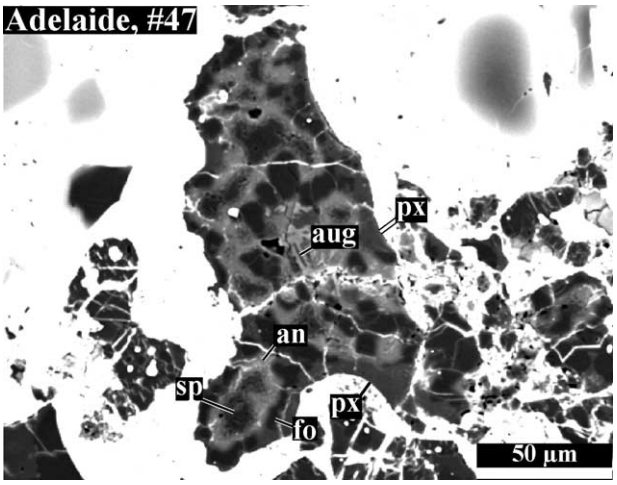

Fig. 10. BSE images of AOA/Al-rich chondrule-like object #47 in Adelaide. It contains several clusters of spinel grains surrounded by anorthitic plagioclase and subhedral forsterite grains. In outer part of the object, forsterite is replaced by pigeonite; in central part, pigeonite is overgrown by augite.

Our petrographic observations suggest the following formation sequence of minerals in AOAs: spinel → melilite → Al-diopside ±spinel ±anorthite; forsterite + FeNi-metal → low-Ca pyroxene. This crystallization sequence is generally consistent with the thermodynamically predicted condensation sequence at $P_{tot} = 10^{-5}$ bar (Fig. 11; Petaev and Wood, 1998): melilite (1503 K), spinel (1371 K), clinopyroxene (1323 K), forsterite (1318 K), anorthite (1293 K), FeNi-metal (1290 K), and orthopyroxene (1263 K) (the appearance of melilite before spinel in the condensation sequence, contrary to petrographic observations, is a well-known problem that has been solved yet; for discussion, see Yoneda and Grossman, 1995; Petaev and Wood, 1998; Ebel and Grosman, 2000). At a total pressure of 10^{-3} bar, the condensation sequence is the same, except the fact that FeNi-metal condenses before forsterite, at 1462 K and 1444 K, respectively (Ebel and Grossman, 2000). Based on these observations, we infer that (i) AOAs are aggregates of gas-solid nebular condensates and possibly igneous CAIs; and (ii) AOAs were not extensively melted after aggregation and can potentially record high-temperature nebular reactions.

4.2. Condensation Reactions Recorded by AOAs

Replacement of melilite by a fine-grained mixture of spinel, Al-diopside and ±anorthite observed in some AOAs (Figs. 1b,c, 2e,f) can be explained by reactions of melilite (gehlenite-åkermanite solid solution) with gaseous Mg and SiO:

$$Ca_2Al_2SiO_{7(s)} + 3SiO_{(g)} + 3Mg_{(g)} + 6H_2O_{(g)} = 2CaMgSi_2O_{6(s)} + MgAl_2O_{4(s)} + 6H_{2(g)} \quad (1)$$

$$Ca_2Al_2SiO_{7(s)} + 3SiO_{(g)} + Mg_{(g)} + 4H_2O_{(g)} = CaAl_2Si_2O_{8(s)} + CaMgSi_2O_{6(s)} + 4H_{2(g)} \quad (2)$$

We note that similar reactions were inferred by Lin and Kimura (1998) to explain replacement of melilite by anorthite and diopside in CAIs in the CV-like chondrite Ninqgiang. Coarse spinel grains in AOAs are commonly corroded to a various degree by the surrounding anorthite (Fig. 3). The observed relationship of spinel and anorthite and the enrichment in Al of diopside towards anorthite can be explained by the following reaction:

$$MgAl_2O_{4(s)} + CaMgSi_2O_{6(s)} + 0.5SiO_{(g)} + 0.5H_2O_{(g)} = 0.5CaAl_2Si_2O_{8(s)} + Mg_2SiO_{4(s)} + 0.5CaAl_2SiO_{6(s)} + 0.5H_{2(g)} \quad (3)$$

According to our thermodynamic calculations (Fig. 11), this reaction will proceed until disappearance of spinel or diopside, which is consistent with the observed variations in modal mineralogy of CAIs in AOAs (Fig. 3). In some cases, the corrosion appearance of spinel and Al-enrichment of diopside towards spinel is observed in nearly complete lack of anorthite

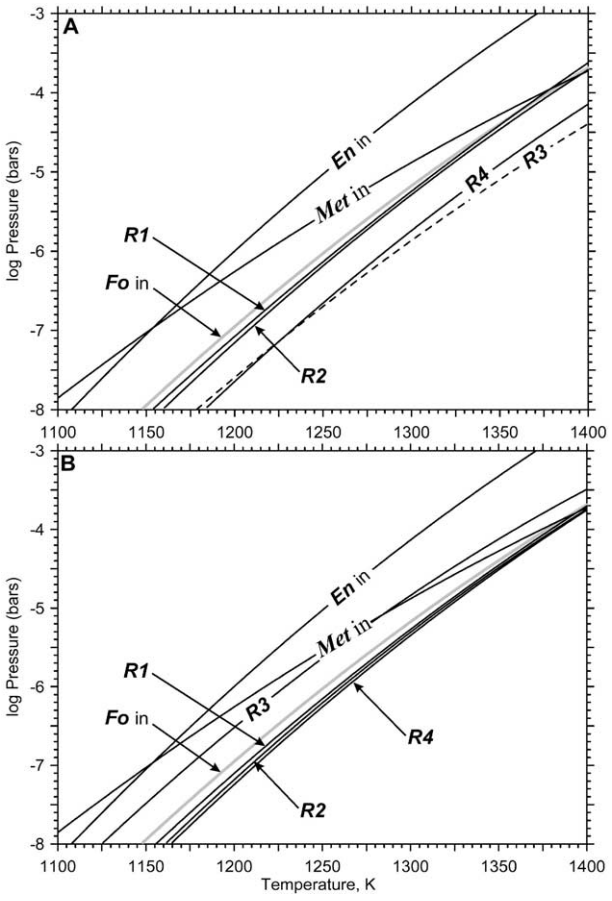

Fig. 11. Equilibrium condensation curves of some minerals and phase boundaries of reactions 1–4 (labeled as R1–R4) equilibrated with the residual nebular gas in a system of the solar composition. Labels on the curves correspond either to the appearance of forsterite (*Fo* in), enstatite (*En* in), and FeNi-metal (*Met* in) or to reaction numbers. The stability fields of melilite are on the right hand sides of the numbered curves. (A) Compositions of coexisting melilite and clinopyroxene are ($Ge_{95}Åk_5$) and ($Di_{95}CATS_5$), respectively. Dashed line shows the boundary of metastable reaction 3. (B) Compositions of coexisting melilite and clinopyroxene are ($Ge_{95}Åk_5$) and ($Di_{80}CATS_{20}$), respectively. For details, see discussion in the text.

(Fig. 4a). These observations can be explained by the reaction involving spinel and melilite:

$$3Ca_2Al_2SiO_{7(s)} + MgAl_2O_{4(s)} + 5SiO_{(g)} + Mg_{(g)} + 6H_2O_{(g)} = [4CaAl_2SiO_6 + 2CaMgSi_2O_6]_{(pxss)} + 6H_{2(g)}. \quad (4)$$

The major component of AOAs, forsterite, certainly formed by direct condensation from nebular gas according to reaction:

$$2Mg_{(g)} + SiO_{(g)} + 3H_2O_{(g)} = Mg_2SiO_{4(s)} + H_{2(g)}. \quad (5)$$

The presence of low-Ca pyroxene replacing forsterite in outer portions of AOAs is consistent with condensation origin of low-Ca pyroxene at relatively low nebular temperatures:

$$Mg_2SiO_{4(s)} + SiO_{(g)} + H_2O_{(g)} = Mg_2Si_2O_{6(s)} + H_{2(g)}. \quad (6)$$

The common occurrences of low-Ca pyroxene rims around FeNi-metal nodules (e.g., Figs. 7c,d) may suggest that Si dissolved in the metal was also involved in the reaction:

$$Mg_2SiO_{4(s)} + Si_{(in\ FeNi)} + 2H_2O_{(g)} = Mg_2Si_2O_{6(s)} + 2H_{2(g)}. \quad (7)$$

We note, however, that the high abundance of low-Ca pyroxene around FeNi-metal, together with the generally low Si content in FeNi-metal condensate (e.g., Petaev et al., 2003), suggest that this reaction is of minor importance in the formation of low-Ca pyroxene in AOAs. Finally, the presence of thick low-Ca pyroxene shells with abundant FeNi-metal nodules around several AOAs (e.g., Figs. 4a–c, 5) may suggest either direct condensation of low-Ca pyroxene and FeNi-metal from the nebular gas:

$$2Mg_{(g)} + 2SiO_{(g)} + 4H_2O_{(g)} = Mg_2Si_2O_{6(s)} + 4H_{2(g)} \quad (8)$$

or formation of this mineral assemblage by reduction of ferrous silicates:

$$2(FeMg)SiO_{4(s)} + 2H_2O_{(g)} = Mg_2Si_2O_{6(s)} + 2Fe_{(s)} + 2H_{2(g)}. \quad (9)$$

Direct condensation of low-Ca pyroxene (reaction 8) is not predicted from a gas of solar composition (e.g., Yoneda and Grossman, 1995; Ebel and Grossman, 2000) and would require existence of fractionated (Mg/Si < solar) gas. Such gas could have resulted from isolation of forsterite either by its physical removal from condensation region or by coarsening of forsterite condensates (Petaev and Wood, 1998; Krot et al., 2003d). This is why we employed CWPI-type condensation which takes into account continuous withdrawal of newly formed condensates from the reactive system by some sort of physical isolation. In the case of AOAs it is their layered texture that results in condensate isolation. Our modeling of disequilibrium condensation in the nebula of solar composition at the isolation degree of 10 rel% per K shows that such a rapid and effective isolation of forsterite (e.g., in AOAs) will result in a large decrease of the Mg/Si ratio in the residual gas, leading to formation of small amounts of low-Ca pyroxene by reaction 6, followed by the direct condensation of low-Ca pyroxene (reaction 8). Reduction of ferrous silicates (reaction 9) is inconsistent with the petrographic observations, including (i) the absence of ferrous silicates associated with CAIs or AOAs in primitive carbonaceous chondrites, (ii) the presence of Ni in metal in low-Ca pyroxene rims, and (iii) the lack of dusty relict grains in these rims.

4.3. Thermodynamic Analysis

We can explore physicochemical conditions of the mineral reactions observed in the AOAs by modeling metasomatic interaction of solid inclusions injected into a system with solar bulk composition. The residual gaseous phase of such a system is assumed to be in equilibrium with the solid phases condensed out of the system. We further assume an open-system type of interaction between the AOAs and the surrounding gaseous phase, i.e., the amounts Si, Mg, Ca, H, and O added to or subtracted from the AOAs by reactions 1- 4 do not change the partial pressures of Ca, Mg, SiO, H_2O, and H_2 in the gaseous system due to very low mass ratio of AOAs to the gaseous phase. The chemical compositions of the residual gaseous phase are calculated using CWPI (condensation with partial isolation) code (Petaev and Wood, 2000; Petaev et al., 2003).

Out of 7 important mineral reactions written above (1–6, 8), reactions 5 and 8 describe direct condensation of forsterite and low-Ca pyroxene from the nebular gas; the P-T conditions of these reactions (and reaction 6) were modeled directly by the CWPI code. Therefore, only reactions 1–4 are included in thermodynamic analysis. The equations linking the equilibrium constants of these reactions (lgK_i) with the partial pressures of gaseous species (lg[Mg], lg[SiO], lg[H_2O/H_2], and lg[Ca]) and activities of end-members of clinopyroxene (lg[Di], lg[CATS]) and melilite (lg[Gel], lg[Åk]) mineral solid solutions are as follows:

$$lgK_1 = 2\,lg[Di] - lg[Gel] - 3\,lg[Mg] - 3\,lg[SiO] - 6\,lg[H_2O/H_2] \quad (10)$$

$$lgK_2 = lg[Di] - lg[Gel] - lg[Mg] - 3\,lg[SiO] - 4\,lg[H_2O/H_2] \quad (11)$$

$$lgK_3 = 0.5\,lg[CATS] - lg[Di] - 0.5\,lg[SiO] - 0.5\,lg[H_2O/H_2] \quad (12)$$

$$lgK_4 = 2\,lg[Di] + 4\,lg[CATS] - 3\,lg[Gel] - 5\,lg[SiO] - lg[Mg] - 6\,lg[H_2O/H_2] \quad (13)$$

Numerical values of equilibrium constants of reactions 1–4 were calculated using the thermodynamic database of the CWPI code. The values of standard thermodynamic properties of minerals and gaseous species involved in the reactions are from Chase et al. (1998), Berman (1988), Sack and Ghiorso (1994), and Robie and Hemingway (1995). The melilite solid solution was treated as nonideal (Charlu et al., 1981). Ignoring small amounts of $MgAl_2SiO_6$, $CaTi^{4+}Al_2O_6$, and $CaTi^{3+}AlSiO_6$, the clinopyroxene was treated as an ideal solution of Ca-Tschermakite (CATS), $CaAl_2SiO_6$, and diopside, $CaMgSi_2O_6$ (Sack and Ghiorso, 1994). Calculations were done in the temperature range of 1000–1600 K and the pressure range of 10^{-3}–10^{-8} bar.

The results of thermodynamic analysis are shown in Figure 11 as the log P vs. T plot. In calculating the positions of phase boundaries on these plots, all parameters of Eqns. 10–13 were replaced with numerical values either calculated using the CWPI code (partial pressures of gaseous species) or measured in the fine-grained inclusions studied. The compositions of mineral solid solutions used in the analysis are Ca-rich melilite ($Ge_{95}Åk_5$), Al-poor diopside ($Di_{95}CATS_5$), and Al-enriched diopside ($Di_{80}CATS_{20}$).

Phase boundaries of the alteration reactions 1–4 are shown at two different compositions of diopside-Al–poor (Fig. 11a) and Al-enriched (Fig. 11b). The major difference between two diagrams is the positions of phase boundaries of reactions 3 and 4 that are highly dependent upon the Al content in diopside. The melilite stability fields are on the right hand side of all phase boundaries. Also plotted are the condensation curves of forsterite (reaction 5), enstatite (reaction 6) and metal which show that the alteration of melilite should occur before the condensation of metal and low-Ca pyroxene. This is consistent with the general absence of both minerals in the refractory component of px-AOAs. Because all phase boundaries are essentially parallel to each other, the alteration sequence is fairly independent of nebular pressure, although the absolute temperatures of the reactions do change.

At the earliest stages of melilite alteration, probably even before the aggregation of CAIs and forsterite into AOAs, the assemblage of melilite and spinel will be replaced by the Al-poor diopside (reaction 4 in Fig. 11a). Because reaction 4 produces twice as much Ca-Tschermakite as diopside, the concentration of the former will gradually increase as reaction 4 proceeds. Given enough time, reaction 4 would be the only alteration reaction until the concentration of Ca-Tschermakite in clinopyroxene increases to >20 mol%, when formation of anorthite by reaction 2 becomes possible. Soon after, a direct replacement of melilite by mixture of diopside and spinel (reaction 1) may occur. At the conditions above reaction 3 is metastable until the appearance of forsterite. However, a wide range of Al_2O_3 concentrations in Al-diopside (Table AE2) suggests that neither reaction has reached an equilibrium state.

If the alteration process has started or continued after the aggregation of the refractory component and forsterite into AOAs, all these reactions can proceed simultaneously until complete disappearance of melilite. After that, only reaction 3 will take place resulting in gradual disappearance of spinel, increase in anorthite abundance, and enrichment of diopside in Al. If reaction 3 is completed, the final equilibrium mineral assemblage of AOAs—forsterite, Al-diopside, and anorthite—would be quite similar (except for small amounts of alkalis, Mn, and SiO_2) to that of Type I chondrules.

Figure 11 clearly shows that the low-Ca pyroxene found in some AOAs formed much later, when the alteration of the refractory component of AOAs was complete (if equilibrium had been reached). The presence of metal in some of the low-Ca pyroxene occurrences in AOAs may suggest that the formation of low-Ca pyroxene occurred at different nebular pressures. In the system of solar composition the forsterite-metal and enstatite-metal reversals occur at nebular pressures of $\sim 10^{-5}$ and $\sim 10^{-7}$ bar (Fig. 11), which define the pressure range of metal-bearing px-AOAs. The metal-free px-AOAs should have formed at lower nebular pressures; however, no such occurrences have been observed yet.

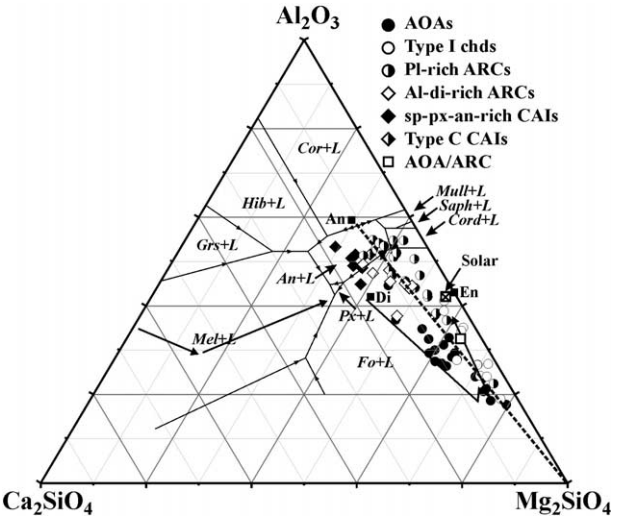

Fig. 12. Bulk compositions of AOAs, igneous (Type C) and nonigneous spinel-pyroxene-anorthite CAIs, Type I ferromagnesian chondrules, Al-rich plagioclase-rich chondrules, and Al-rich Al-diopside-rich chondrules, projected from spinel onto the plane Ca_2SiO_4-Mg_2SiO_4-Al_2O_3 (MacPherson and Huss, 2003). Data from Jones and Scott (1989), Sheng et al. (1991), Komatsu et al. (2001), Krot and Keil (2002), Krot et al. (2001b, 2002a, 2003a; this study).

4.4. Genetic Relationship between Refractory Inclusions and Chondrules: Evidence of AOAs with Low-Ca Pyroxene

Bulk compositions of AOAs are rather similar to magnesian (Type I and Al-rich) chondrules, suggesting possible genetic relationship between objects (MacPherson and Huss, 2000). In Figure 12, representing a projection from spinel onto the plane Ca_2SiO_4-Mg_2SiO_4-Al_2O_3 (MacPherson and Huss, 2000), we plotted bulk compositions of AOAs, igneous (Type C) and nonigneous spinel-pyroxene-anorthite CAIs, and Type I (Jones and Scott, 1989) and Al-rich chondrules from Acfer 094 (Krot et al., 2003), Adelaide (Krot et al., unpublished), CRs (Weber and Bischoff, 1997; Krot and Keil, 2002; this study), CBs (Krot et al., 2001a), and CVs (Sheng et al., 1991; Krot et al., 2002a). Based on the mineralogy, the Al-rich chondrules are divided into plagioclase-rich and Al-diopside-rich. The plagioclase-rich chondrules consist of olivine and low-Ca pyroxene phenocrysts, plagioclase laths, and silica-pyroxene-plagioclase mesostasis (Krot and Keil, 2002). The Al-diopside-rich chondrules consist of Al-diopside, spinel, forsterite, and minor anorthitic mesostasis (Krot et al., 2001a,b, 2002b, 2003a). On this diagram, bulk compositions of AOAs can be explained as a mixture of spinel-pyroxene-anorthite CAIs and forsterite. The Al-diopside-rich chondrules are compositionally similar to spinel-pyroxene-anorthite CAIs and AOAs, and hence could have been produced by melting of these objects. In contrast, bulk compositions of AOAs and Type I and plagioclase-rich chondrules plot on different sides of anorthite-forsterite thermal

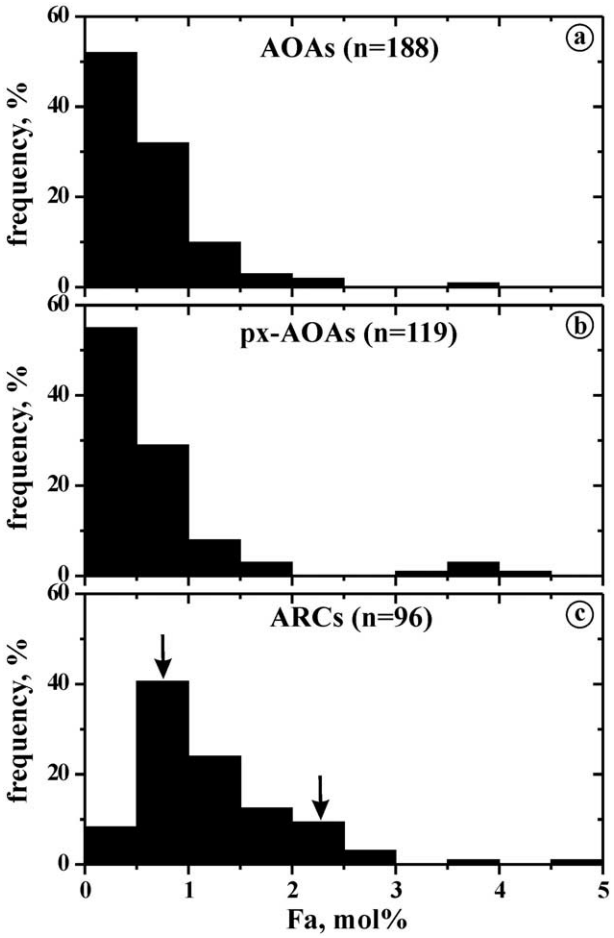

Fig. 13. Histograms of fayalite content in olivines in (a) AOAs, (b) AOAs with low-Ca pyroxene, and (c) in Al-rich plagioclase-rich chondrules (ARCs) in carbonaceous chondrites.

divide, suggesting that these chondrules cannot be produced from AOAs by an igneous fractionation. A similar conclusion was reached by Komatsu et al. (2001), based on the differences in mineral chemistry of AOAs and Al-rich chondrules. Formation of low-Ca pyroxene by reaction of AOAs with gaseous SiO or melting of AOAs surrounded by a dust of solar composition moves bulk compositions of the AOAs towards enstatite, across the thermal divide, providing possible mechanisms of transformation of refractory objects into magnesian and plagioclase-rich chondrules. The latter mechanism is supported by the presence of AOA/Al-rich chondrule-like objects containing abundant low-Ca pyroxene and/or pigeonite in their peripheries (Figs. 9, 10) and having bulk and mineral compositions similar to chondrules (Figs. 12–16).

The relatively rare occurrences of low-Ca pyroxene in AOAs may indicate that either AOAs were isolated (removed) from the hot nebular gas before condensation of low-Ca pyroxene, e.g., by a magnetocentrifugally driven stellar wind (Shu et al., 1996, 1997, 2001) or by a turbulent diffusion (Cuzzi et al., 2003), or that gas-solid condensation of low-Ca pyroxene by reaction of forsterite and gaseous SiO was kinetically inhibited (Imae et al., 1993; Komatsu et al., 2001). Isolation of refractory inclusions from high temperature nebular gas may be required to explain the survival of the corundum-, hibonite-, and melilite-rich CAIs in different chondrite groups (Krot et al., 2002b; Simon et al., 2002). However, the lack of kinetic information on reactions of these refractory minerals with nebular gas makes this hypothesis difficult to test. In contrast, Imae et al. (1993) showed experimentally that reaction between solid forsterite and gaseous SiO is kinetically controlled and sluggish. The lack of low-Ca pyroxene in many AOAs containing significant Mn contents in forsterite (e.g., Fig. 14; Weisberg et al., 2003) is also consistent with slow kinetics of solid forsterite-gaseous SiO reaction, because Mn is predicted to condense after condensation of enstatite (e.g., Yoneda and Grossman, 1995; Ebel and Grossman, 2000). Although the kinetic reasons may explain rare occurrences of AOAs with low-Ca pyroxene, the presence of low-Ca pyroxene in $\geq$ 10% of all AOAs and substantial replacement of forsterite by low-Ca pyroxene in some AOAs (e.g., Figs. 2c,f, 6b, 7b) appear to contradict the kinetic constraints. Slow kinetics of solid forsterite-gaseous SiO reaction could be overcome, if reactive forsterite was enclosed in silicate melt. Petrographic evidence for melting of many AOAs with low-Ca pyroxene (Table 1) might support this mechanism.

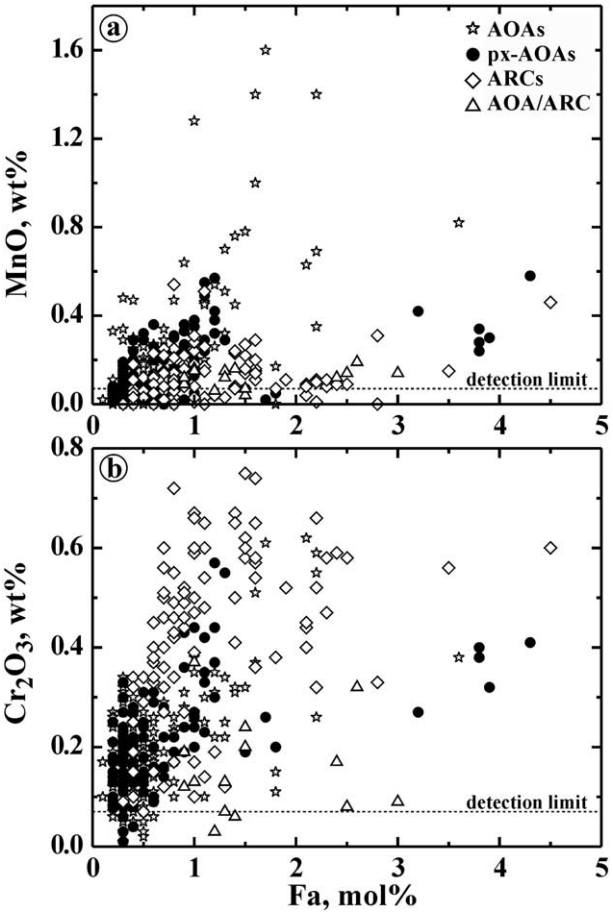

Fig. 14. Fayalite vs. MnO (a) and Cr_2O_3 (b) in olivines in AOAs with and without low-Ca pyroxene and in Al-rich plagioclase-rich chondrules in carbonaceous chondrites.

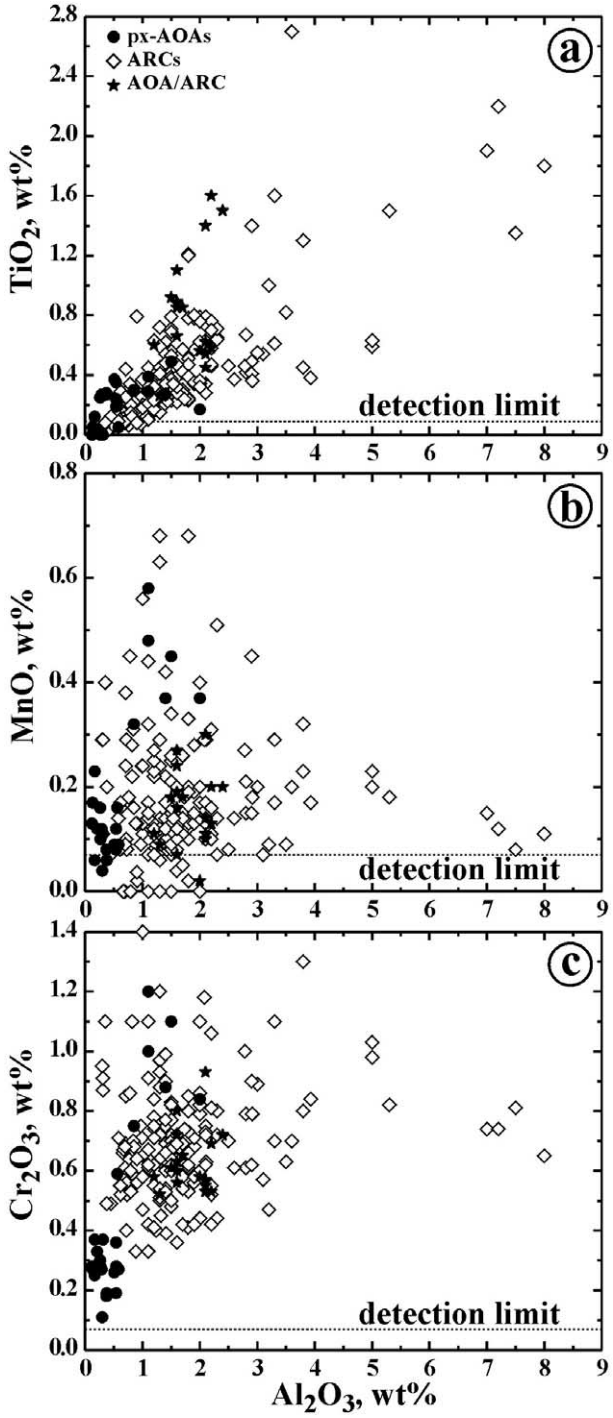

Fig. 15. Al_2O_3 vs. TiO_2 (a), MnO (b) and Cr_2O_3 (c) in low-Ca pyroxenes in AOAs, Al-rich plagioclase-rich chondrules (ARC), and AOA/ARC-like objects in carbonaceous chondrites.

4.5. AOAs with Low-Ca Pyroxene: Implications for Chondrule Formation

Chondrules are believed to have formed by flash-melting of solid precursors. The rare occurrences of low-Ca pyroxene in AOAs in carbonaceous chondrites together with kinetic constraints on enstatite formation by replacement of forsterite (Imae et al., 1993) are difficult to reconcile with the common presence of low-Ca pyroxene-rich Type I chondrules in carbonaceous chondrites (e.g., Grossman et al., 1988). If condensation origin of enstatite by replacement of forsterite was limited, the origin of pyroxene-rich magnesian chondrules requires either direct condensation of low-Ca pyroxene from fractionated

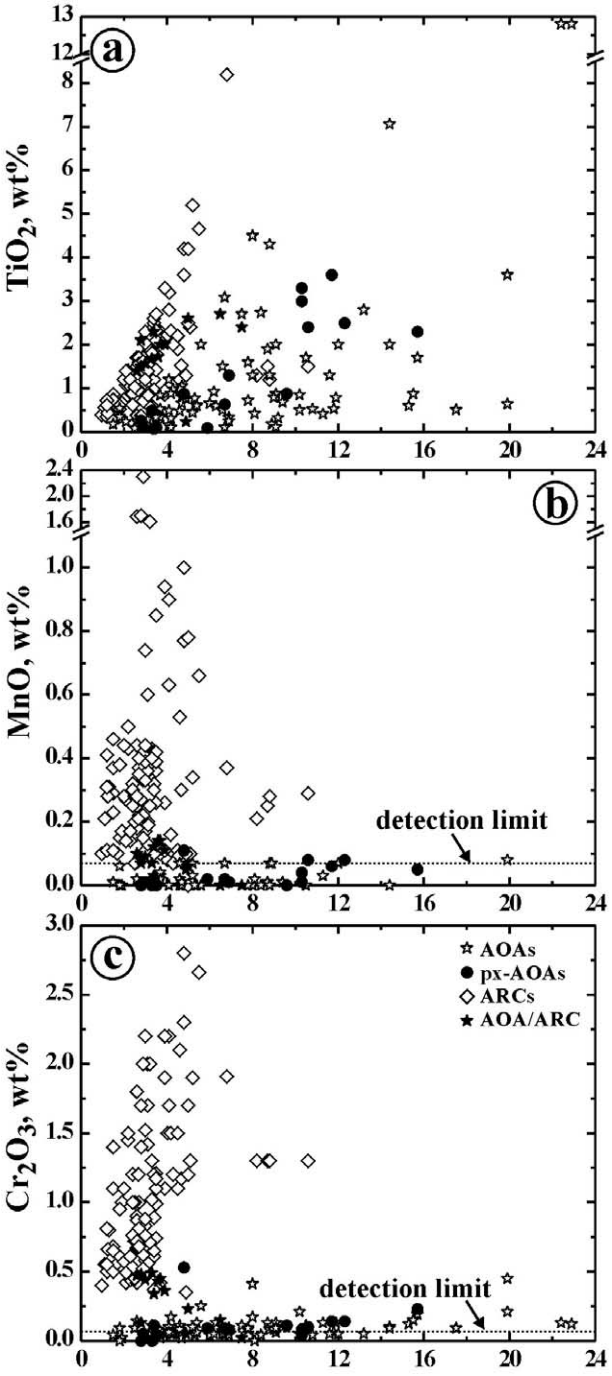

Fig. 16. Al_2O_3 vs. TiO_2 (a), MnO (b) and Cr_2O_3 (c) in high-Ca pyroxenes in AOAs with and without low-Ca pyroxene, Al-rich plagioclase-rich chondrules (ARCs), and AOA/ARC-like objects in carbonaceous chondrites.

nebular gas (Mg/Si ratio less than solar) or condensation of gaseous SiO into chondrule melts (Ebel and Grossman, 2000; Tissandier et al., 2002), or a disequilibrium, CWPI-type condensation of chondrule precursors. Formation of Type I chondrules (or their immediate precursors) in CR chondrites from fractionated nebular gas has been recently proposed by Krot et al. (2000, 2003d) and Palme and Klerner (2000).

5. CONCLUSIONS

AOAs in primitive carbonaceous chondrites consist of forsterite ($Fa_{<2}$), FeNi-metal, and a refractory component (fine-grained minerals and individual CAIs) composed of Al-diopside, anorthite, ±spinel, and exceptionally rare melilite ($Åk_{<15}$); some CAIs in AOAs have compact, igneous textures. Melilite in AOAs is replaced by a fine-grained mixture of spinel, Al-diopside, and anorthite. Spinel is corroded by anorthite or by Al-diopside. In ~10% of > 500 AOAs studied in the CR, CV, CM, CO, CH, CB, and ungrouped carbonaceous chondrites Acfer 094, Adelaide, and LEW85332, forsterite is replaced to a various degree by low-Ca pyroxene; in some cases, low-Ca pyroxene contains abundant tiny inclusions of FeNi-metal grains. Some of the AOAs with low-Ca pyroxene show evidence for melting of various degrees. In the most extensively melted AOA in the CV chondrite Leoville, only spinel grains are relict; forsterite, anorthite and Al-diopside were melted. This AOA has a thick igneous shell of low-Ca pyroxene with abundant FeNi-metal nodules and is texturally similar to a Type I chondrule.

Based on these observations and thermodynamic analysis, we conclude that AOAs are aggregates of solar nebular condensates that originated in ^{16}O-rich gaseous reservoir(s) (Krot et al., 2002c). Some of the CAIs were melted before aggregation into AOAs. After aggregation, most AOAs must have experienced only incipient melting. Before and possibly after aggregation, melilite and spinel reacted with the gaseous SiO and Mg to form Ca-Tschermakite ($CaAl_2SiO_6$)-diopside ($CaMgSi_2O_6$) solid solution and anorthite. Forsterite in some AOAs reacted with gaseous SiO in the CAI- or chondrule-forming regions to form low-Ca pyroxene: $Mg_2SiO_{4(s)} + SiO_{(g)} + H_2O_{(g)} = Mg_2Si_2O_{6(s)} + H_{2(g)}$. Some pyroxenes may have formed by oxidation of Si dissolved in FeNi-metal: $Mg_2SiO_4 + Si_{(in\ FeNi)} + 2H_2O_{(g)} = Mg_2Si_2O_6 + 2H_{2(g)}$ or by direct gas-solid condensation: $Mg_{(g)} + SiO_{(g)} + H_2O_{(g)} = Mg_2Si_2O_{6(s)} + H_{2(g)}$, but these mechanisms seem to be of limited importance.

Although bulk compositions of AOAs are rather similar to those of Type I chondrules, on a projection from spinel onto the plane Ca_2SiO_4-Mg_2SiO_4-Al_2O_3, these objects plot on different sides of the anorthite-forsterite thermal divide, suggesting that Type I chondrules cannot be produced from AOAs by an igneous fractionation. Formation of low-Ca pyroxene by reaction of AOAs with gaseous SiO or melting of AOAs surrounded by a dust of solar composition moves bulk compositions of the AOAs towards chondrules, and provides possible mechanisms of transformation of refractory materials into chondrules or chondrule precursors.

The rare occurrences of low-Ca pyroxene in AOAs may indicate that either AOAs were isolated from the hot nebular gas before condensation of low-Ca pyroxene or that condensation of low-Ca pyroxene by reaction between forsterite and gaseous SiO was kinetically inhibited. If the latter is correct, then the common occurrences of pyroxene-rich Type I chondrules may require either direct condensation of low-Ca pyroxenes from fractionated nebular gas or condensation of gaseous SiO into chondrule melts.

Acknowledgments—This work was supported by NASA grants NAG5-10610 and NAG5-12882 (A. N. Krot, P.I.), NAG5-4212 (K. Keil, P.I.), NAG5-10484 (S. B. Jacobsen, P.I.), and Monkasho grants (H. Yurimoto, P.I.). We thank Dr. Y. Lin, Dr. M. Weisberg, Dr. S. Russell, and the anonymous reviewer for helpful comments and suggestions. This is Hawaii Institute of Geophysics and Planetology publication No. 1319 and School of Ocean and Earth Science and Technology publication No. 6340.

Associate editor: S. S. Russell

REFERENCES

Aléon J., Krot A. N., and McKeegan K. D. (2002) Ca-Al-rich inclusions and amoeboid olivine aggregates from the CR carbonaceous chondrites. *Meteorit. Planet. Sci.* **37,** 1729–1755.

Bar-Matthews M., MacPherson G. J., and Grossman L. (1979) An SEM-petrographic study of amoeboid olivine aggregates in Allende (abstract). *Meteoritics* **14,** 342.

Berman R. G. (1988) Internally-consistent thermodynamic data for minerals in the system Na_2O-K_2O-CaO-MgO-FeO-Fe_2O_3-Al_2O_3-SiO_2-TiO_2-H_2O-CO_2. *J. Petrol.* **29,** 445–522.

Charlu T. V., Newton R. C., and Kleppa O. J. (1981) Thermochemistry of synthetic $Ca_2Al_2SiO_7$ (gehlenite)-$Ca_2MgSi_2O_7$ (åkermanite) melilites. *Geochim. Cosmochim. Acta* **45,** 1609–1617.

Chase M. W. Jr. (1998) NIST-JANAF *Thermodynamic Tables*. 4th ed. Monograph No. 9. J. Phys. Chem. Ref. Data.

Chizmadia L. J., Rubin A. E., and Wasson J. T. (2002) Mineralogy and petrology of amoeboid olivine inclusions in CO3 chondrites; relationship to parent-body aqueous alteration. *Meteorit. Planet. Sci.* **37,** 1781–1796.

Cohen R. E., Kornacki A. L., and Wood J. A. (1983) Mineralogy and petrology of chondrites and inclusions in the Mokoia CV3 chondrite. *Geochim. Cosmochim. Acta* **47,** 1739–1757.

Cuzzi J. N., Davis S. S., and Dobrovolskis A. R. (2003) Formation and distribution of CAIs in the protoplanetary nebula (abstract). *Lunar Planet. Sci.* **34,** 1749.

Ebel D. S. and Grossman L. (2000) Condensation in dust-enriched systems. *Geochim. Cosmochim. Acta* **64,** 339–366.

Davy R., Whitehead S. G., and Pitt G. (1978) The Adelaide meteorite. *Meteoritics* **13,** 121–139.

Fitzgerald M. J. and Jones J. B. (1977) Adelaide and Bench Crater—Members of a new subgroup of the carbonaceous chondrites. *Meteoritics* **12,** 443–458.

Greshake A. (1997) The primitive matrix components of the unique carbonaceous chondrite Acfer 094: A TEM study. *Geochim. Cosmochim. Acta* **61,** 437–452.

Grossman L. and Steele I. M. (1976) Amoeboid olivine aggregates in the Allende meteorite. *Geochim. Cosmochim. Acta* **40,** 149–155.

Grossman J. N., Rubin A. E., Nagahara H., and King E. A. (1988a) Properties of chondrules. In *Meteorites and the Early Solar System* (eds. J. F. Kerridge and M. S. Mathews), pp. 619–659. University of Arizona Press.

Hashimoto A. and Grossman L. (1987) Alteration of Al-rich inclusions inside amoeboid olivine aggregates in the Allende meteorite. *Geochim. Cosmochim. Acta* **51,** 1685–1704.

Hiyagon H. and Hashimoto A. (1999) ^{16}O excesses in olivine inclusions in Yamato-86009 and Murchison chondrites and their relation to CAIs. *Science* **283,** 828–831.

Huss G. R. and Hutcheon I. D. (1992) Abundant $^{26}Mg^*$ in Adelaide refractory inclusions (abstract). *Meteoritics* **27,** 236.

Hutcheon I. D. and Steele I. M. (1982) Refractory inclusions in the Adelaide carbonaceous chondrite (abstract 1441). *Lunar Planet. Sci.* **23,** 352–353.

Imae N., Tsuchiyama A., and Kitamura M. (1993) An experimental study of enstatite formation reaction between forsterite and Si-rich gas. *Earth Planet. Sci. Lett.* **118,** 21–30.

Imai H. and Yurimoto H. (2003) Oxygen isotopic distribution in an amoeboid olivine aggregate from the Allende CV chondrite: Primary and secondary processes. *Geochim. Cosmochim. Acta* **67,** 765–772.

Itoh S., Rubin A. E., Kojima H., Wasdson J. T., and Yurimoto H. (2002) Amoeboid olivine aggregates and AOA-bearing chondrule from Y-81020 CO 3.0 chondrite: Distribution of oxygen and magnesium isotopes (abstract). *Lunar Planet. Sci.* **33,** 1490.

Jones R. H. and Scott E. R. D. (1989) Petrology and thermal history of type IA chondrules in the Semarkona (LL3.0) chondrite. *Proc. Lunar Planet. Sci. Conf.* **19,** 523–536.

Kallemeyn G. W. and Wasson J. T. (1982) The compositional classification of chondrites; III. Ungrouped carbonaceous chondrites. *Geochim. Cosmochim. Acta* **46,** 2217–2228.

Kerridge J. J. (1985) Carbon, hydrogen and nitrogen in carbonaceous chondrites; abundances and isotopic compositions in bulk samples. *Geochim. Cosmochim. Acta* **49,** 1707–1714.

Komatsu M., Krot A. N., Petaev M. I., Ulyanov A. A., Keil K., and Miyamoto M. (2001) Mineralogy and petrography of amoeboid olivine aggregates from the reduced CV3 chondrites Efremovka, Leoville and Vigarano: Products of nebular condensation and accretion. *Meteorit. Planet. Sci.* **36,** 629–643.

Kornacki A. S. and Wood J. A. (1984a) Petrography and classification of Ca, Al-rich and olivine-rich inclusions in the Allende CV3 chondrite. *J. Geophys. Res.* **89,** B573–B587.

Kornacki A. S. and Wood J. A. (1984b) The mineral chemistry and origin of inclusion matrix and meteorite matrix in the Allende CV3 chondrite. *Geochim. Cosmochim. Acta* **48,** 1663–1676.

Krot A. N. and Keil K. (2002) Anorthite-rich chondrules in CR and CH carbonaceous chondrites: Genetic link between Ca, Al-rich inclusions and ferromagnesian chondrules. *Meteorit. Planet. Sci.* **37,** 91–111.

Krot A. N., Weisberg M. K., Petaev M. I., Keil K., and Scott E. R. D. (2000) High-temperature condensation signatures in Type I chondrules from CR carbonaceous chondrites (abstract). *Lunar Planet. Sci.* **31,** 1470.

Krot A. N., McKeegan K. D., Russell S. S., Meibom A., Weisberg M. K., Zipfel J., Krot T. V., Fagan T. J., and Keil K. (2001a) Refractory Ca, Al-rich inclusions and Al-diopside-rich chondrules in the metal-rich chondrites Hammadah al Hamra 237 and QUE 94411. *Meteorit. Planet. Sci.* **36,** 1189–1217.

Krot A. N., Hutcheon I. D., and Huss G. R. (2001b) Aluminum-rich chondrules and associated refractory inclusions in the unique carbonaceous chondrite Adelaide (abstract). *Meteorit. Planet. Sci.* **36,** A105–A106.

Krot A. N., Hutcheon I. D., and Keil K. (2002a) Anorthite-rich chondrules in the reduced CV chondrites: Evidence for complex formation history and genetic links between CAIs and ferromagnesian chondrules. *Meteorit. Planet. Sci.* **37,** 155–182.

Krot A. N., Meibom A., Weisberg M. K., and Keil K. (2002b) The CR chondrite clan. Implications for early solar system processes. *Meteorit. Planet. Sci.* **37,** 1451–1490.

Krot A. N., McKeegan K. D., Leshin L. A., MacPherson G. J., and Scott E. R. D. (2002c) Existence of an ^{16}O-rich gaseous reservoir in the solar nebula. *Science* **295,** 1051–1054.

Krot A. N., Fagan T. J., Keil K., McKeegan K. D., Sahijpal S., Hutcheon I. D., Petaev M. I. and Yurimoto H. (2003a) Ca, Al-rich inclusions, amoeboid olivine aggregates and Al-rich chondrules from the unique carbonaceous chondrite Acfer 094: I. Mineralogy and petrology. *Geochim. Cosmochim. Acta*, in press.

Krot A. N., Petaev M. I., Itoh S., Fagan T. J., Yurimoto H., and Russell S. S. (2003b) Amoeboid olivine aggregates in carbonaceous chondrites: Records of nebular and asteroidal processes. *Geochim. Cosmochim. Acta* **67,** A237.

Krot A. N., Petaev M. I., Russell S. S., Itoh S., Fagan T. J., Yurimoto H., and Keil K. (2003c) Amoeboid olivine aggregates in primitive carbonaceous chondrites: Records of high-temperature nebular processing (abstract). *Meteorit. Planet. Sci.* **38 (***Suppl.***)**, A74.

Krot A. N., Libourel G., Goodrich C. A., Pataev M. I., and Killgore M. (2003d) Silica-rich igneous rims around magnesian chondrules in CR carbonaceous chondrites: Evidence for Fractional condensation during chondrule formation (abstract). *Lunar Planet. Sci.* **34,** CD-ROM #1451.

Lin Y. and Kimura M. (1998) Anorthite-spinel-rich inclusions in the Ningqiang carbonaceous chondrite: Genetic links with Type A and C inclusions. *Meteorit. Planet. Sci.* **33,** 435–446.

Lin Y. and Kimura M. (2003) Ca-Al-rich inclusions from the Ningqiang meteorite: Continuous assembalges of nebular condensates and genetic link to Type B inclusions. *Geochim. Cosmochim. Acta* **67,** 2251–2267.

MacPherson G. J., Bar-Matthews M., Tanaka T., Olsen E., and Grossman L. (1983) Refractory inclusions in the Murchison meteorite. *Geochim. Cosmochim. Acta* **47,** 823–839.

MacPherson G. J. and Huss G. R. (2000) Convergent evolution of CAIs and chondrules: Evidence from bulk compositions and a cosmochemical phase diagram (abstract). *Lunar Planet. Sci.* **31,** CD-ROM #1796.

McSween H. Y., Jr.. (1977) Chemical and petrographic constraints on the origin of chondrules and inclusions in carbonaceous chondrites. *Geochim. Cosmochim. Acta* **41,** 1843–1860.

Newton J., Bischoff A., Arden J. W., Franci I. A., Geriger T., Greshake A., and Pillinger C. T. (1995) Acfer 094, a uniquely primitive carbonaceous chondrite from the Sahara. *Meteoritics* **30,** 47–56.

Palme H. and Klerner S. (2000) Formation of chondrules and matrix in carbonaceous chondrites (abstract). *Meteorit. Planet. Sci.* **35,** A124.

Petaev M. I. and Wood J. A. (1998) The condensation with partial isolation (CWPI) model of condensation in the solar nebula. *Meteorit. Planet. Sci.* **33,** 1123–1137.

Petaev M. I. and Wood J. A. (2000) The condensation origin of zoned metal grains in Bencubbin/CH-like chondrites: Thermodynamic model (abstract). *Lunar Planet. Sci.* **31,** 1608.

Petaev M. I., Wood J. A., Meibom A., Krot A. N., and Keil K. (2003) The ZONMET thermodynamic and kinetic model of metal condensation. *Geochim. Cosmochim. Acta* **67,** 1737–1751.

Robie R. A. and Hemingway B. S. (1995) Thermodynamic properties of minerals and related substances at 298.15 K and 1 bar (10^5 pascals) pressure and at higher temperatures. *USGS Bull.* 2131.

Rubin A. E. (1998) Correlated petrologic and geochemical characteristics of CO3 chondrites. *Meteorit. Planet. Sci.* **33,** 385–391.

Sack R. O. and Ghiorso M. S. (1994) Thermodynamics of multicomponent pyroxenes. III. Calibration of $Fe^{2+}(Mg)_{-1}$, $TiAl_2(MgSi_2)_{-1}$, $TiFe^{3+}{}_2(MgSi_2)_{-1}$, $AlFe^{3+}(MgSi)_{-1}$, $NaAl(Ca,Mg)_{-1}$, $Al_2(Mg)Si)_{-1}$ and $Ca(Mg)_{-1}$ exchange reactions between pyroxenes and silicate melts. *Contrib. Mineral. Petrol.* **118,** 271–296.

Sheng Y. J., Hutcheon I. D., and Wasserburg G. J. (1991) Origin of plagioclase-olivine inclusions in carbonaceous chondrites. *Geochim. Cosmochim. Acta* **55,** 581–599.

Shu F. H., Shang H., and Lee T. (1996) Toward and astrophysical theory of chondrules. *Science* **271,** 1545–1552.

Shu F. H., Shang H., Glassgold A. E., and Lee T. (1997) X-rays and fluctuating x-winds from protostars. *Science* **277,** 1475–1479.

Shu F. H., Shang H., Gounelle M., Glassgold A. E., and Lee T. (2001) The origin of chondrules and refractory ionclusions in chondritic meteorites. *Astrophys. J.* **548,** 1029–1070.

Simon S. B., Davis A. M., Grossman L., and McKeegan K. D. (2002) A hibonite-corundum inclusion from Murchison: A first generation condensate from the solar nebula. *Meteorit. Planet. Sci.* **37,** 533–548.

Tissandier L., Libourel G., and Robert F. (2002) Gas-melt interactions and their bearings on chondrule formation. *Meteorit. Planet. Sci.* **37,** 1377–1389.

Weber D. (1995) Refractory inclusions from the carbonaceous chondrite Acfer 094 (abstract). *Meteorit. Planet. Sci.* **30,** 595–596.

Weber D. and Bischoff A. (1997) Refractory inclusions in the CR chondrite Acfer 059-El Djouf 001: Petrology, chemical composition, and relationship to inclusion populations in other types of carbonaceous chondrites. *Chem. Erde.* **57,** 1–24.

Weisberg M. K. and Prinz M. (1990) Refractory inclusions in CR2 (Renazzo-type) chondrites (abstract). *Lunar Planet. Sci.* **21,** 1315–1316.

Weisberg M. K., Connolly H. C., Jr., and Ebel D. S. (2003) Amoeboid olivine aggregates in CR chondrites (abstract). *Lunar Planet. Sci.* **34,** 1513.

Yoneda S. and Grossman L. (1995) Condensation of CaO-MgO-Al_2O_3-SiO_2 liquids from cosmic gases. *Geochim. Cosmochim. Acta* **59,** 3413–3444.